Buoyancy and Shear Characteristics of Hurricane-Tornado Environments

EUGENE W. MCCAUL, JR.

National Center for Atmospheric Research, Boulder, Colorado*

(Manuscript received 30 July 1990, in final form 14 February 1991)

ABSTRACT

Detailed composite profiles of temperature, moisture, and wind are constructed for tornado environments in tropical cyclones that affected the United States during the period 1948–86. Winds are composited in components radial and tangential to the tropical cyclone center at observation time. Guided by observed patterns of tornado occurrence, composites are constructed for a variety of different stratifications of the data, including proximity to tornadoes, position relative to the cyclone center, time of day, time after cyclone landfall, cyclone translation speed, and location of landfall. The composites are also compared to composite soundings from Great Plains tornado environments. A variety of sounding parameters are examined to see which are most closely related to the patterns of tornado distribution.

Lower-tropospheric vertical shears are generally stronger in the tropical cyclone tornado environments than on the Great Plains. Vertical shear and helicity parameters, along with 700-hPa wind speed, show the best correlations with the reported intensity of the tropical cyclone tornado outbreaks. Buoyancy for the tropical cyclone tornado cases is much smaller than that seen with Great Plains tornado events and shows a weak negative correlation with tornado outbreak severity.

Composite thermal and wind profiles computed in each quadrant relative to cyclone motion reveal distinct signatures, with relatively small thermal instability near the cyclone centers and enhanced shear and helicity in the tornado-prone right front quadrant. The patterns of wind profile differences from quadrant to quadrant resemble those that would result from the interaction of the cyclone with a steering current containing unidirectional shear that is roughly parallel to the direction of cyclone motion.

The number and intensity of tropical-cyclone–spawned tornadoes are generally found to increase with increasing cyclone intensity and size. Cyclone translation speed is not well correlated with tornado productivity. Although most tornadoes occur on the day of cyclone landfall, some cyclones are able to maintain wind shear profiles that are favorable for tornadic storm development through several days after landfall. Atlantic coast cyclones produce fewer tornadoes than their counterparts from the Gulf of Mexico, in part apparently as a result of a deficiency in postlandfall exposure of the right-front quadrant to land.

1. Introduction

McCaul (1987) has pointed out that high values of storm-relative streamwise vorticity (Davies-Jones 1984) and relative helicity (Lilly 1986) occurred in the environmental wind profiles of the 1985 Hurricane Danny tornado outbreak and that supercell convection appeared to have been responsible for at least some of the observed tornado families that occurred. Novlan and Gray (1974) reported composite thermal and wind profiles for United States hurricane-tornado cases between 1948 and 1972. Their results, however, came too early to be scrutinized in the light of such parameters as helicity and streamwise vorticity, which have only recently been used to explain rotation in severe storm updrafts. Davies-Jones (1984) has shown that storm-relative streamwise vorticity is abundant in many Great Plains tornadic environments. Davies-Jones et al. (1990), examining a sample of Great Plains tornadoes, have argued that storm-relative total helicity is a good predictor of tornado intensity. Weisman and Klemp (1982; 1984) have related convective available potential energy (CAPE), ambient vertical shear, and bulk Richardson number (BRN) to modes of convection in numerical simulations initiated with soundings more or less representative of Great Plains severe storm cases.

In order to study the extent to which such parameters apply to tornadoes and tornadic convection within tropical cyclone environments, and to compare the tropical cyclone tornado cases with previously documented Great Plains cases, an extensive new composite study of the hurricane environments has been conducted. This study takes advantage of a much larger dataset than any used in previous studies and allows construction of a tornado proximity sounding that is more detailed and specific to the environment of the

* The National Center for Atmospheric Research is sponsored by the National Science Foundation.

Corresponding author address: Dr. Eugene W. McCaul, Jr., Universities Space Research Association, NASA/MSFC ES-43, Huntsville, AL 35812.

tropical-cyclone–spawned tornadic storms. In addition, a variety of other composite soundings have been computed in an attempt to examine the differential distribution of conditions within the tornado-producing tropical cyclone and to compare variations in these conditions with variations in the observed temporal and spatial distributions of tornadoes. Among the conditions examined in these composites are azimuth and range relative to the cyclone center, translation speed of the cyclone, location of landfall, time of day, and time after cyclone landfall.

The remainder of this paper is organized into four major parts. Section 2 gives pertinent details of the data processing and analysis procedures. Section 3 contains statistical descriptions of the data, followed by a series of composite soundings. These results are discussed in section 4, and a summary and recommendations for future work are given in section 5.

2. Data analysis

This study makes use of all available sounding data taken in "tropical cyclone environments" that were associated with documented tornadoes in the United States during the years 1948–86. Tropical cyclone environments were taken to be those associated with any North Atlantic cyclone listed on the National Hurricane Center hurricane tape (the "HURDAT" tape), and thus consisted of full-fledged hurricanes, tropical storms and depressions, and a few subtropical cyclones. Tornadoes were found to occur in association with each of these cyclone types. Although this study was not restricted to fullfledged hurricanes, subsequent references to the HURDAT cyclones will be made using the generic term "hurricanes" for convenience.

To establish which North Atlantic hurricanes affected United States rawinsonde observation (raob) sites during the period 1948–86, reported hurricane positions from the HURDAT tape (for the period 1948–85) and from *Storm Data* (for 1986) were compared with a listing of positions and periods of operation of 162 United States raob sites. Tornado reports were obtained from the National Severe Storms Forecast Center (NSSFC) tornado tape (1950–85), *Monthly Climatological Summaries* (1948–49), and *Storm Data* (1986). The hurricane and tornado databases were compared to produce a list of hurricane tornado events during 1948–86. Tornadoes occurring within 800 km of the center of a storm on the HURDAT tape were considered hurricane-tornado candidates. Daily weather maps were inspected for these events and tornado cases corresponding more to frontal or other nonhurricane influences were excluded from consideration.

The resulting list of tornadoes was then examined to determine which events were close to raob sites, using the proximity criteria of 3 h and 185 km employed by Novlan and Gray (1974). This procedure reduced the size of the tornado list by almost a factor of two. The time series raob database at the National Center for Atmospheric Research (NCAR) was then searched to create a collection of all the available raobs at the tornado-proximal raob sites at the times of the tornadoes and also for one day prior to and following the events. The raob data were examined and edited to remove errors. All reported winds were transformed into radial ($U = V_r$) and tangential ($V = V_\theta$) components in a stationary coordinate frame centered on the hurricane, whose position at the time of the raob was estimated using the HURDAT tape data.

The set of 1296 soundings that came out of this procedure included 199, which, according to the Novlan and Gray (1974) proximity criteria, were actually associated with tornado activity. These tornadic raobs were made in 68 of the 87 different tornado-producing hurricanes that affected the United States during the years covered by this study. Another 48 hurricanes occurring during those years produced no reported tornadoes and their sounding data are not considered in this study. The database consists of raobs from 79 of the 90 separate hurricane landfalls that produced tornadoes. The total number of hurricane-spawned tornadoes reported in the 87 hurricanes was 626, while the number of tornadoes proximal to the raobs in the database was 366.

Composite soundings presented in this paper consist of two basic types. In the first type, a composite sounding is created by averaging sets of raobs that satisfy only the rather loose proximity criteria of Novlan and Gray (1974). These "general proximity" composites are useful in studying temporal and spatial patterns of thermodynamic and kinematic conditions within the tornadic hurricanes. The second type of composite is created using only those few raobs satisfying a very selective set of proximity criteria designed to identify raobs that were taken in "inflow" conditions near the tornadic convective storms. The composite resulting from application of these restrictive criteria is called the "close proximity" composite. A detailed description of the close proximity criteria is given in section 3c.

The actual composite calculations consisted of transformation of the raob data to sigma coordinates, followed by averaging at the surface and at an additional 100 equal increments of sigma aloft, followed by a remapping of the averaged results back to pressure coordinates using the mean of the reported station pressures. For each composite constructed, the variances of temperature, dewpoint, and wind components were also computed for each of the 101 levels, so as to permit assessment of the statistical significance of patterns appearing within and among the various composites. To avoid biasing the results, soundings made in rapid sequence at one station, and showing little difference from one another, were limited to one sounding per 6 h. Also excluded were soundings with

data not reaching at least 300 hPa or containing large data gaps.

In addition to the computation of the composites, maps of sounding-derived parameters such as CAPE, BRN, 0–6 km vertical shear of layer-averaged winds used in computing BRN (termed here "0–6 km BRN shear" to avoid ambiguity), storm cell-relative total helicity, relative helicity, and streamwise vorticity were plotted for the entire set of raobs. CAPE, BRN shear, and BRN were evaluated according to the methods of Weisman and Klemp (1982) to facilitate comparison with other work. Mathematically, the cell-relative total helicity is defined (Lilly 1986) as $H_t = (\mathbf{V} - \mathbf{V}_c) \cdot (\mathbf{k} \times \partial\mathbf{V}/\partial z)$, the relative helicity as $H_r = H_t/[|\mathbf{V} - \mathbf{V}_c| |\partial\mathbf{V}/\partial z|]$, and streamwise vorticity as $\omega_s = H_t/|\mathbf{V} - \mathbf{V}_c|$, where $\mathbf{V}$ is the ground-relative flow, $\mathbf{V}_c$ is cell motion, and $\mathbf{k}$ is the unit vector along the vertical (z) coordinate. Each of the estimates of H_t, H_r, and ω_s cited here are computed by averaging the profiles of point estimates of the desired quantity over either the lowest 3, 6, or 12 km.

The cell-relative helicity and streamwise vorticity calculations require assessment of motions $\mathbf{V}_c$ of convective cells, data that are not generally available. For the purposes of this study, cell motions were assumed to be identical to the 0–6 km mass-weighted mean winds. Because cell motions often differ from these mean winds, the helicity calculations do not generally give results equal to the true helicity values and should therefore perhaps be termed "pseudohelicity." However, throughout this paper the terms helicity and streamwise vorticity will be used for convenience. The relative helicity, total helicity, and streamwise vorticity estimates will also be referred to collectively as "helicity estimates." These estimates of helicity and related parameters are intended mainly to diagnose hodograph shape and curvature. As McCaul (1987) pointed out, this technique of estimating helicity is likely to produce values of relative helicity that underestimate the true values. Experience has shown that for strongly curved hodographs the helicity estimates presented here should be increased by 20%–50% to obtain values corresponding to realistic storm motions. Estimates of the augmented 0–3 km total helicity so obtained can be converted to the units used by Davies-Jones et al. (1990) by multiplying by the depth of the averaging layer, 3000 m.

For the purposes of some of the data stratifications, it was necessary to know the time and location of hurricane landfall points. Landfall time was defined here to be the date and time at which the center of a hurricane crossed a "smoothed" coastline. This definition of landfall excluded traversals by a hurricane center of the Florida Keys, Cape Hatteras, Cape Cod, or the extreme southeastern tip of the Mississippi delta. Landfall times were estimated from careful inspection of the tracks of the hurricanes, as depicted in "Tropical Cyclones of the North Atlantic Ocean, 1871–1986" (U.S. Dept. of Commerce 1987). For landfalls that occurred at a small incidence angle, took place at slow translational speeds, or involved abrupt directional changes, additional searches were made of the available literature (primarily *Monthly Weather Review, Storm Data,* and *Weatherwise*) to confirm and refine the landfall time estimates. Experience has shown that the estimates of landfall time used here are generally accurate to within 2 h.

The general proximity dataset is large enough to permit not only one-way, but sometimes two-way, stratifications of the data for compositing purposes. For instance, it is possible to construct general proximity composite soundings for both "fast-moving" and "slow-moving" hurricanes. It is not possible, however, to construct such composites for any arbitrary "quadrant" of the fast-moving hurricanes, because such a two-way stratification would, in general, yield too small a data sample for a meaningful composite. Fortunately, however, most of the raobs come from the right-front quadrants of hurricanes, so that it is in fact possible to construct a two-way composite for right-front quadrant data. Extensive use is made of this property of the data in the construction of composite profiles presented in sections 3c–j.

The data sample considered in this study, although large, is limited by the fact that only tornado-producing hurricanes are included. In addition, because only those raob sites, which were at some time proximal to a tornado during the nearby passage of a hurricane, were examined here, the sample of soundings obtained for this study does not constitute the entirety of raobs that were made even in the tornado-producing hurricanes. The present raob data are therefore not adequate to address questions about intrinsic differences between tornadic and nontornadic hurricanes. Nevertheless, inspection of the temporal patterns in the raob time series suggests that the general-proximity composites do in fact accurately reflect the variations of the real meteorological conditions within the hurricanes. Furthermore, because the majority of United States hurricane landfalls result in tornadoes, it is strongly suspected that the composites presented here describe accurately some of the basic aspects of landfalling hurricanes in general, even those that fail to produce tornadoes.

3. Results

a. Overall characteristics of hurricane-tornado outbreaks

As a starting point, it is appropriate to summarize some of the general characteristics of hurricane tornado outbreaks. In the 39-yr data sample examined here, approximately 59% of all the landfalls produced at least one tornado. Some of these tornadoes were spawned as long as five or more days after landfall, although the

rate of production was quite small after the third day. The number of tornadoes reported with hurricanes is most often only one or two, although this survey identified 113 associated with Hurricane Beulah in 1967. The number distribution of tornado production by the hurricanes in the data sample is shown in Table 1.

The data in Table 1 suggest that it is possible to classify hurricane tornado outbreaks as either "minor" (not more than 8 tornadoes), "major" (more than 8 tornadoes), or "severe" (more than 24 tornadoes). Under this classification, there have been 18 major hurricane tornado outbreaks in the period 1948–86, four of which were severe. These 18 outbreaks have been responsible for 413 of the 626 tornadoes (66%) spawned by the hurricanes in the present data sample. Their conditions are documented in 99 of the 199 tornadic raobs (50%). Additional statistical data on the characteristics of tornado-producing hurricanes and on the temporal-spatial distributions of the tornadoes are presented in the subsections below.

b. *Dependence of sounding parameters on position relative to hurricane center*

As a first step in the data analysis, maps were made of the azimuth–range dependence of various parameters derived from the individual soundings. Some of the patterns found in this exercise formed the basis for many data stratifications employed in constructing the various general proximity composites to be described later. The maps are drawn in a polar coordinate system that is hurricane-relative; i.e., oriented such that the 360° azimuth always corresponds to the direction in which the hurricane was moving. Thus the 0°–90° quadrant in figures described in this subsection actually corresponds to the "right-front" quadrant of the hurricane.

TABLE 1. Distribution of number of tornadoes in landfalling hurricanes.

NT	NH	Hurricane names/years (major outbreaks only)
0	48	
1	18	
2	18	
3	7	
4	8	
5	7	
6	6	
7	5	
8	0	
9	1	Isbell (64)
10	4	Hilda (64), Frederic (79), Subtrop.1 (82), Elena (85)
11	1	Juan (85)
12	1	Cleo (64)
13	0	
14	1	Babe (77)
15	0	
16	2	Candy (68), Edith (71)
17	1	Agnes (72)
18	0	
19	0	
20	1	Carla (61)
21	1	Audrey (57)
22	1	Alicia (83)
29	1	Allen (80)
34	1	David (79)
39	1	Danny (85)
113	1	Beulah (67)

NT = number of tornadoes associated with a hurricane.
NH = number of hurricanes producing NT tornadoes.

The spatial distribution of F-scale sum per raob, defined for each raob as the sum over all reported proximal tornadoes of unity plus the Fujita F-scale value (Fujita 1973), is shown in Fig. 1a. The F-scale numbers range from F-0 to F-5 and are designed to correspond to surface windspeeds as large as 32, 50, 70, 92, 116, and 142 m s^{-1}, respectively. Raobs not proximal to any reported tornadoes, but which are used in evaluating the spatial distribution of various raob parameters, are also shown in the figure. Their F sum is specified to be zero. The F sum is taken to be roughly representative of the intensity of hurricane tornado activity that can be studied with the present raob data.

Figure 1a shows that most of the tornado-proximal data were taken in the right quadrants of the hurricanes, with an especially heavy concentration of data in the right-front quadrant. This is in agreement with all previous studies. In addition, the largest concentration of large circles also occurs in the right-front quadrant, indicating that the raobs proximal to severe hurricane-tornado outbreaks most often were located in that quadrant. Most of the raobs associated with the severe outbreaks occurred in the 200–400 km range interval. Very few hurricane-tornado raobs were made more than 200 km to the left of the hurricane track.

Figure 1b shows a contour plot of gridded, objectively analyzed values of the F sum. In the objective analysis, a distance weighting function with spatial cutoff of 200 km was employed to interpolate the actual observed data to a uniform 100-km grid. Contours were then drawn for those regions having sufficient data to ensure representativeness. The pattern of contours in Fig. 1b closely mirrors the pattern seen in Fig. 1a. Throughout the rest of this subsection, plots of contoured, objectively analyzed data will be used to describe the spatial variation of the other raob parameters.

It is expected that many errors exist in the assigned F-scale values of the various tornadoes (Doswell and Burgess 1988), but because some meteorological parameters show significant correlations with the F-scale data, they probably reflect the tornado outbreak severity reasonably accurately in a statistical sense. The F sum is, therefore, also used as a basis for studying correlations between tornado outbreak severity and various raob-derived meteorological parameters. However, only tornado-proximal raobs (i.e., those having nonzero F sum) are used in these correlation calculations. This is done not only because the number

of nonproximity raobs is large enough to bias the results, but also because all the raobs in this study, even those not in proximity to tornadoes, come from tornadic hurricanes. Thus, in looking for correlations between tornado outbreak severity and intensity of meteorological parameters, only the question of tornado severity, not the question of tornado occurrence or nonoccurrence, can properly be addressed.

Although F sum appears to be adequate as a measure of the local severity of a hurricane-tornado outbreak, its distribution is highly skewed toward small values, making it unsuitable for direct use in parametric tests of statistical significance. To reduce this skewness, the logarithm of F-scale sum is taken as the measure of outbreak intensity associated with each raob. Except for BRN, and to a lesser extent CAPE, the raob-derived meteorological parameters were approximately normally distributed. Thus, cross correlations between log(F sum) and various meteorological parameters could be computed and their significance assessed using standard parametric statistical techniques, such as t tests. In computing the correlations, all raobs meeting the criteria outlined earlier were used and were assumed to be independent data. The adequacy of this assumption was examined by computing additional correlations using only one raob per station per hurricane. These yielded correlations not greatly different, so that serial correlation did not appear to have much impact on the results. In addition, significance levels obtained from the t tests agree very well with those estimated from simulations of the correlation distributions derived from many random reshufflings of the log(F sum) data.

In Figs. 2–7 are shown the spatial distributions of CAPE, BRN shear, BRN, and 0–3 km H_r, H_t, and ω_s, drawn relative to the hurricane centers. The patterns of BRN shear and the helicity parameters more closely resemble that of log(F sum) than do those of CAPE or BRN. Average CAPEs reach a minimum of less than 400 J kg^{-1} near and just to the left of the hurricane centers, relative to their motion. CAPE reaches a maximum well to the right of the hurricane track and is generally larger to the rear of the hurricane than it is to the forward side. The shear and helicity parameters, on the other hand, reach distinct maxima in the right-front or right quadrants. The occurrence of maximum shear in these areas is roughly consistent with the findings of Novlan and Gray (1974; Figs. 10, 12).

Table 2 gives a summary of cross-correlation coefficients between a selection of important raob parameters and log(F sum). As an aid in evaluating the data in the table, it is noted that the results of the t tests and correlation simulations show that correlations of approximately 0.14 are significant at the 5% level (i.e., have only a 5% chance of occurring due to random effects). As expected from inspection of Figs. 1b–7, the parameters that correlate best with tornado outbreak severity are the helicity parameters and BRN shear. Interestingly, the helicity parameters averaged through 12 km show the highest correlations, ranging from 0.31 to 0.34, even though the mean values of the helicity parameters attain their highest values in the 0–3 km layer. This suggests that favorable shears in deeper layers are important for development of hurricane-spawned tornadic storms. Among the more straightforward parameters tested, the 700-hPa wind speed had the highest correlation, 0.31. This is comparable in magnitude to the correlations achieved by the 0–12 km helicity parameters. CAPE shows a weak negative correlation of −0.07 with log(F sum). Such a correlation is significant at approximately the 23% level. Because of this negative correlation between CAPE and tornado outbreak severity, soundings having zero CAPE were not automatically excluded from this database. However, exclusion of the zero-CAPE soundings from the computations causes no significant impact on the correlation results.

Although all the highest ranking correlations are statistically significant at better than the 1% level, their absolute magnitudes are not very large. Possible reasons for the smallness of the correlations include (a) mesoscale variability of the data, with potentially important variations having amplitudes not much larger than the accuracy of raob measurements; (b) errors in F-scale assignments and probable under-reporting of the tornadoes; (c) for the helicity parameters, errors in the estimates of storm cell motions; and (d) inherently limited predictability of details of tornado intensity using larger scale ambient single-parameter data.

c. *Hurricane-tornado proximity composites*

The first task to be addressed by the compositing effort was the identification of the essential overall features of the thermal and wind profiles in the hurricane-tornado environment. This task was accomplished by computing a composite using a few carefully selected raobs taken in very close proximity to hurricane-tornado events. Only soundings made within 2 h and 40 km of a hurricane-spawned tornado were used in constructing this "close proximity" composite. In addition, soundings used in this composite were required to have been made in locations that, taking observed hurricane translation into account during the time interval between the tornado and raob time, lay at larger radii from the hurricane centers than the corresponding tornado reports to which they were proximal. This latter restriction was designed to ensure that the raobs were made on the outer side of any rainbands in which the tornadoes were embedded. It was assumed that the boundary layer air on the outer side of the convective bands is representative of the air flowing into the updrafts of the tornadic storms. The number of raobs satisfying these restrictive selection criteria was 10.

The composite of these 10 raobs is shown in Fig. 8, which depicts the results in skew T–log p, and polar

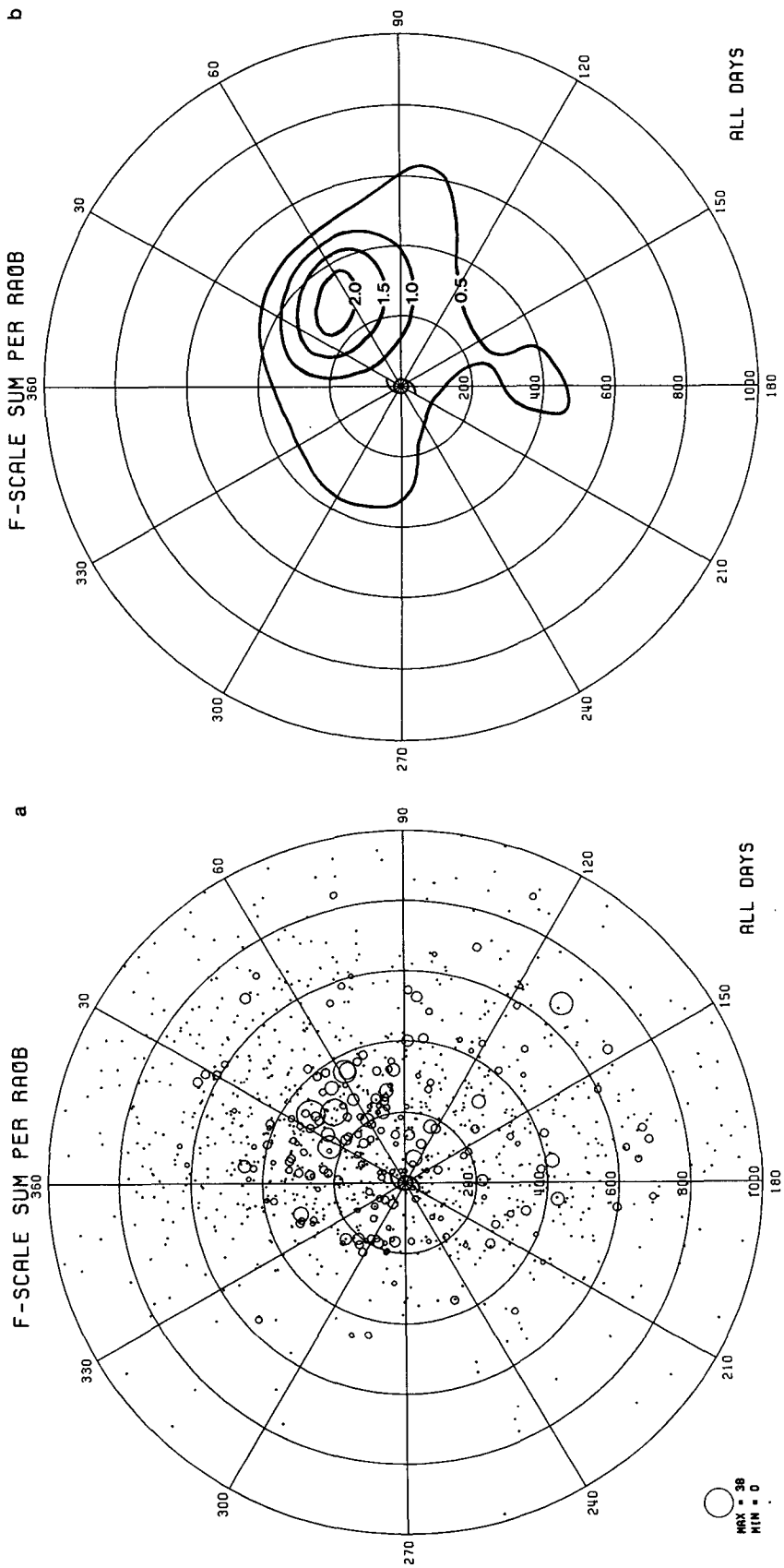

FIG. 1. Spatial distributions, relative to hurricane motion, of (a) values of raw F-scale sum per raob for full set of 1296 raobs and (b) objectively analyzed values of F-scale sum per raob for the same data. Areas of circles in (a) are proportional to F sum, with raobs not proximal to tornadoes shown as dots. Objective analysis grid mesh in (b) is spaced at 100-km intervals. In both diagrams, the hurricane is at the center and is moving toward 360°. Range rings, labeled along the 180° azimuth, are 200 km apart.

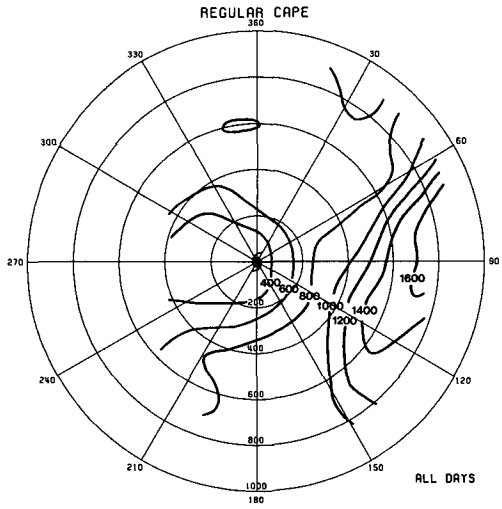

FIG. 2. Spatial distribution of CAPE for the 1296 hurricane raobs. Format is as in Fig. 1b. Units of contours are joules per kilogram.

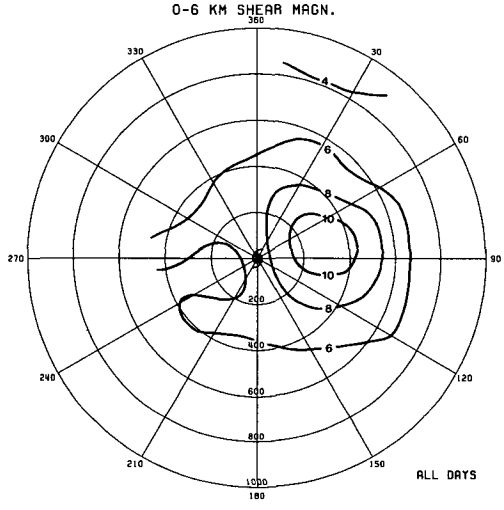

FIG. 3. Spatial distribution of 0–6 km "BRN shear" magnitude (see text) for the 1296 hurricane raobs. Format is as in Fig. 1b. Units of contours are meters per second.

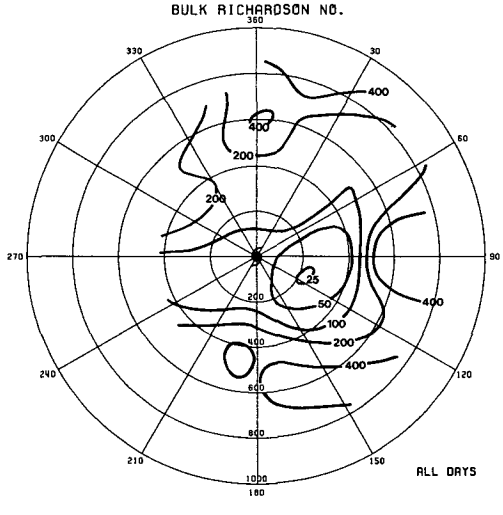

FIG. 4. Spatial distribution of bulk Richardson number for the 1296 hurricane raobs. Format is as in Fig. 1b. Units of contours are dimensionless.

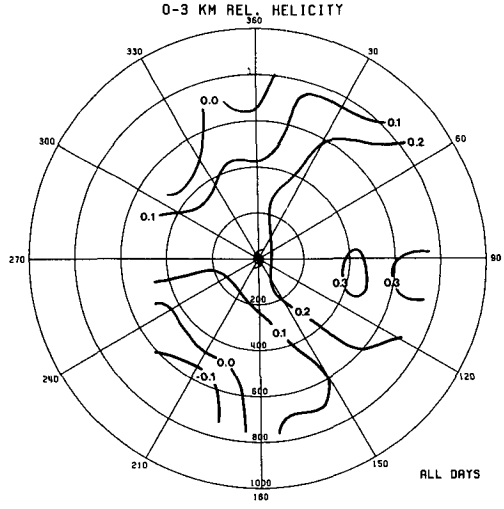

FIG. 5. Spatial distribution of 0–3 km relative helicity H_r for the 1296 hurricane raobs. Format is as in Fig. 1b. Units of contours are dimensionless.

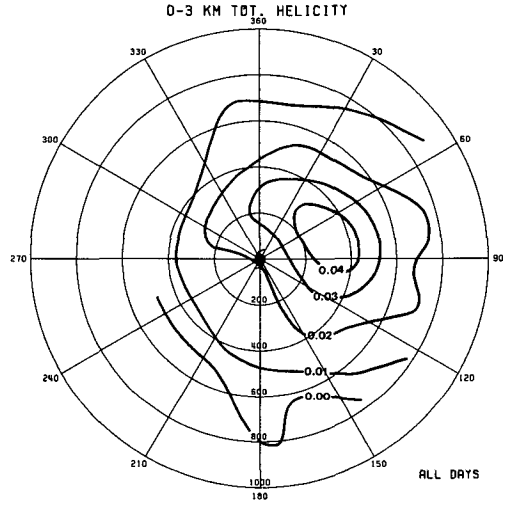

FIG. 6. Spatial distribution of 0–3 km total helicity H_t for the 1296 hurricane raobs. Format is as in Fig. 1b. Units of contours are meters per second squared.

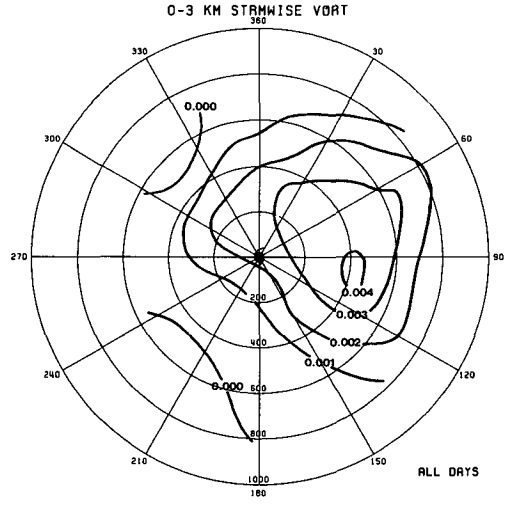

FIG. 7. Spatial distribution of 0–3 km streamwise vorticity ω_s for the 1296 hurricane raobs. Format is as in Fig. 1b. Units of contours are inverse seconds.

hodograph format. The temperature profile features a conditionally unstable layer below approximately 650 hPa, surmounted by an absolutely stable layer. Above 500 hPa the lapse rate is close to moist adiabatic. Relative humidities are high throughout much of the troposphere, with dewpoint depressions often less than 6°C. Maximum buoyancies of boundary layer parcels are achieved around 650 hPa. The tropopause is quite high, lying on average near 150 hPa. These patterns resemble those found by Sheets (1969). The winds are characterized by inflow toward the hurricane center below approximately 2 km altitude, with outflow above. The hodograph shows a distinct "loop" or "horseshoe" shape, with veering winds and shears from the surface through 10 km and beyond. The strongest winds occur near 2–3 km altitude. Very strong vertical shears exist in the lowest 1 km. These results are consistent with those of Novlan and Gray (1974), but show more detail and demonstrate clearly how the wind profile is organized relative to the hurricane center.

It is noteworthy that the altitude of maximum tangential winds, near 2–3 km, is almost twice that observed in mature maritime hurricanes (Frank 1977, Fig. 9). There is evidently an increase in the depth of the layer containing positive shear of the tangential wind following landfall. This redistribution of tangential momentum may be due to the postlandfall adiabatic core cooling of the hurricane described by Novlan and Gray (1974) or the increasing influence of surface friction (Gentry 1983).

Also shown in Fig. 8 is the general-proximity composite of all the available raobs, taken without regard to radial position relative to the tornadic storms. Comparison of the two composite profiles in Fig. 8 shows many similarities, but also a significant increase in windspeed and shear for the close proximity case. In addition, temperatures in the close-proximity composite are slightly warmer in the middle and upper troposphere and slightly cooler below 700 hPa. The relatively small difference in the mean radial distances of the two Fig. 8 composites from the hurricane centers (266.9 km for close, 337.8 km for general) cannot explain all the differences between the composite profiles. The close-proximity winds are stronger most likely because they come from within and near the rainbands in the right-front quadrants of relatively intense hurricanes, while the general proximity winds come from a variety of quadrants in both weak and intense hurricanes. The differences in the temperature profiles can also be attributed in part to differences in hurricane intensity. The dependences of the kinematic and thermodynamic fields on hurricane-relative azimuth and hurricane intensity are discussed in more detail below.

TABLE 2. Cross correlations between log(F sum) and raob parameters using only raobs in general proximity to tornadoes.

Variable	Correlation with log(F sum)	t value
CAPE (J kg^{-1})	−0.07	−0.91
BRN shear (m s^{-1})	0.32	4.47
Bulk Richardson number	−0.18	−2.50
0–3 km H_r	0.16	2.18
0–6 km H_r	0.22	3.04
0–12 km H_r	0.31	4.34
0–3 km H_t (m s^{-2})	0.26	3.58
0–6 km H_t (m s^{-2})	0.28	3.99
0–12 km H_t (m s^{-2})	0.32	4.51
0–3 km ω_s (s^{-1})	0.26	3.54
0–6 km ω_s (s^{-1})	0.30	4.18
0–12 km ω_s (s^{-1})	0.34	4.77
850 hPa wind speed (m s^{-1})	0.22	3.08
700 hPa wind speed (m s^{-1})	0.31	4.40
500 hPa wind speed (m s^{-1})	0.25	3.46
Sfc–850 hPa shear (m s^{-1})	0.19	2.54
Sfc–700 hPa shear (m s^{-1})	0.28	3.92
Sfc–500 hPa shear (m s^{-1})	0.20	2.69

Table 3 contains summary listings of the values of mean CAPE, BRN shear, BRN, and layer-averaged H_r, H_t, and ω_s for 0–3, 0–6, and 0–12 km layers of the soundings used in generating each composite. CAPE and BRN are much smaller and the shear and helicity parameters much larger for the close proximity data. Mean total helicity converted to the form used by Davies-Jones et al. (1990) is approximately 300 J kg^{-1} for the close proximity composite. This value is near the threshold for "strong" (at least F-2 intensity) tornadoes.

For the purpose of quantitatively describing the statistical variability of the composites, the standard deviations (rms) of the raob variables were examined. In general, the rms profiles (not shown) are rather similar to those of Oklahoma severe squall line environments (Bluestein and Jain 1985). The rms variability of the temperature of the general proximity composite data is on the order of 2°C, while that for dewpoint is near 2°C at the surface, growing to approximately 7°C at midlevels. The rms variability of the tangential wind component increases from just under 4 m s^{-1} near the surface to approximately 10–12 m s^{-1} in the upper troposphere; the corresponding figures for the radial wind component average about 20% smaller. Although these rms velocity variations appear large, they represent the full range of windspeeds encompassed in the entire set of hurricane-tornado proximity raobs, in the absence of any stratification of the data. Most of the composites based on data stratifications described in later subsections feature reduced rms variability of the winds.

Using the computed rms profiles and a level-by-level count of the number of observations comprising each composite, it was possible to construct 95% confidence limits for each profile variable. The fluctuations embodied by these confidence limits were generally about 0.4°C for temperature, 0.4°–1.0°C for dewpoint, and 0.6–2.0 m s^{-1} for each of the wind components. Because the general-proximity composite in Fig. 8 was constructed from a much larger sample, its rms profiles

were used as the basis for a z-test statistical comparison with the close-proximity composite. The analysis confirms that the winds in the close-proximity profile are significantly stronger through much of the troposphere than those of the general-proximity profile. The significance level of the differences is often 1% or better. The temperature profile of the close proximity composite is significantly cooler at low levels and warmer in the upper troposphere than that of the general proximity profile. Dewpoints in the midtroposphere are significantly greater for the close-proximity profile.

Although the composite hurricane-tornado environmental profiles of Fig. 8 show well-defined structure, it is worth noting that some individual hurricane tornado soundings deviated noticeably from the composite profiles. CAPEs ranged from 0 to more than 3000 J kg^{-1}, and maximum winds were under 10 m s^{-1} in strength in some of the soundings. However, the soundings with weak winds were never associated with more than one or two weak tornadoes; all the major tornado outbreaks occurred in environments having wind maxima in excess of 15 m s^{-1}.

The mean hurricane-tornado proximity sounding and hodograph are rather different from their tornado proximity counterparts on the Great Plains. These differences are highlighted in Fig. 9, which shows the close-proximity hurricane-tornado profiles along with the Oklahoma supercell mean profiles of Bluestein and Jain (1985). The latter profiles closely approximate the findings of other composite tornado proximity studies (Maddox 1976; Darkow and McCann 1979; Schaefer and Livingston 1988) and are thus taken to be representative of tornadic environments on the Great Plains. The hodographs can only be compared in a general way, because the winds in the Oklahoma profile were composited using true zonal and meridional components.

With respect to the thermal data, the hurricane-tornado events display much less CAPE than the Oklahoma events. The mean of the close proximity hurricane-tornado CAPEs (Table 3) is 253 J kg^{-1}, or only about 10% of the 2542 J kg^{-1} value found by Bluestein and Jain (1985; Table 3) for Oklahoma supercells. The hurricane CAPEs are comparable in magnitude to those found by Barnes and Stossmeister (1986) near the rainbands of a maritime hurricane. Surface wet-bulb potential temperatures θ_w are 22.7°C in the Oklahoma composite and 22.3°C in the hurricane composite, but the temperature and dewpoint profiles are otherwise rather different. Most prominent among the differences are the extensive dry layer aloft, the layer of enhanced static stability below 700 hPa, and the steep lapse rates in the Oklahoma composite.

Much of the CAPE in the hurricane-tornado cases is realized in the conditionally unstable layer that exists between the surface and about 600 hPa. Boundary layer parcels ascending through this layer can achieve buoyancies of 2°–3°C, thanks to a minimum in ambient saturation wet-bulb potential temperature θ_w^* that occurs near 650 hPa. This relatively "cool" layer is apparently created by the hurricane's own circulation, which draws in unperturbed lower-tropospheric tropical air, while warming the middle and upper troposphere with the anvils from intense hurricane-core convection. Thus it is apparently not the lower troposphere that is being cooled, but rather the middle and upper troposphere that are being warmed. This warming and attendant reduction of CAPE contribution aloft is most pronounced in intense hurricanes, which, it will be shown, are just the ones most likely to produce large tornado outbreaks (with large F sums) after landfall.

The changes to the mid- and upper-level temperature and moisture profiles wrought by the hurricanes can be seen by comparing the hurricane profile with that of Jordan's (1958) mean Atlantic hurricane season sounding, shown in Fig. 10. The hurricane temperature profile is slightly cooler than the Jordan profile below 600 hPa, but becomes 2°–3°C warmer aloft. The dewpoint profiles are virtually identical below about 850 hPa. The absence of any significant evidence of mid-level drying, both in the composites and in the individual soundings, suggests that subsidence does not play a major role in producing this warming aloft. Notwithstanding the increased overall moisture in the hurricane sounding, the CAPE decreases from 1345 J kg^{-1} in the Jordan profile to the hurricane value of 253 J kg^{-1}. This residual lower-tropospheric minimum in θ_w^* and warm layer aloft have also been observed in reconnaissance flight soundings taken in maritime hurricanes (see, e.g., Hawkins and Imbembo 1976, Figs. 5, 6, and 10), in other mean hurricane soundings (Sheets 1969), and in the hurricane-tornado study of Novlan and Gray (1974).

With respect to the shears, the hurricane-tornado close proximity composite displays greater magnitude, at least at low levels, than the Oklahoma supercell composite. Wind vector magnitude differences between the surface and 1 km are 14.8 m s^{-1} for the hurricane profile and 9.0 m s^{-1} for the Oklahoma profile. In terms of BRN shear, the Oklahoma profile yields 12.5 m s^{-1} of shear and the hurricane profile 14.0 m s^{-1}. Taking into account the smaller CAPE and larger shears found in the close proximity hurricane tornado cases, it is found that the BRN of the hurricane cases (3.3) is much smaller than that of the Great Plains tornado cases (32.8). For both datasets the BRN falls in the "possible supercell" range (Weisman and Klemp 1982, 1984).

d. Azimuthal variations around the hurricanes

In Fig. 1 it was shown that most of the raobs associated with intense tornado activity in landfalling hurricanes occur in the right-front quadrants of the hurricanes. A map of the positions of all 626 documented

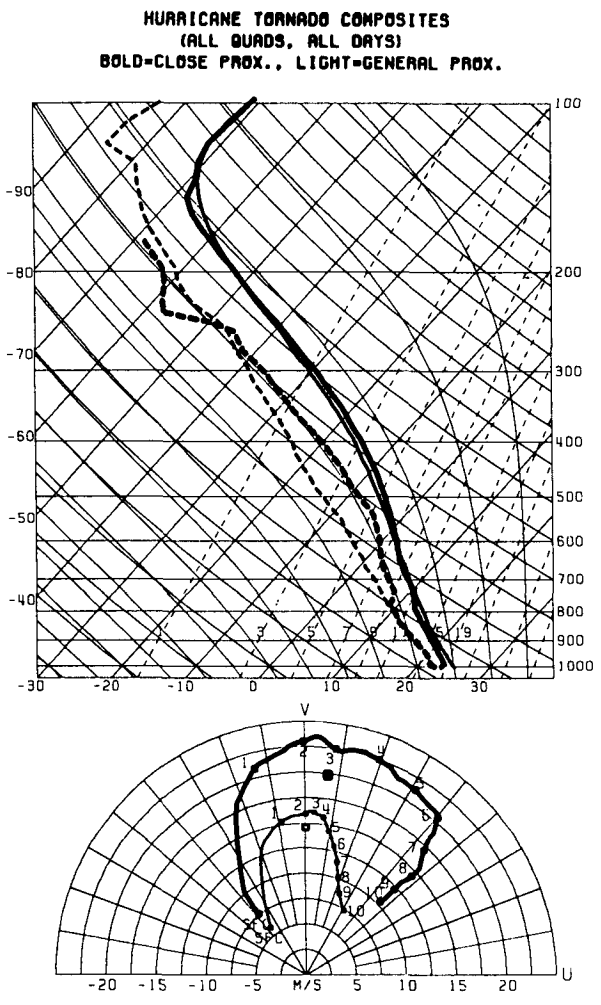

FIG. 8. Skew T–log p and hodograph diagrams for the composite soundings taken in close proximity (heavier lines) and general proximity (lighter lines) to hurricane tornado events. The U and V components represent the radial and tangential winds relative to hurricane centers at raob time. Boxes on hodograph diagrams mark 0–6 km mean winds used as estimates of convective cell motion.

tornadoes occurring in the period 1948–86 echoes this pattern (Fig. 11). Insofar as the mean heading of landfalling hurricanes in this study is nearly due north, this pattern would appear as a preference for tornadoes in the northeast quadrants of hurricanes if the tornado data were plotted relative to true north. The preference for tornado activity in the northeast quadrants of landfalling hurricanes has been documented by Hill et al. (1966), Novlan and Gray (1974), and Gentry (1983).

To investigate the strong preference for hurricane tornado formation in the right-front quadrants of hurricanes, composite profiles were constructed in each of the quadrants relative to calculated hurricane motion. The composites in the four quadrants were also averaged, using unit weighting for each quadrant's composite, to produce an azimuthally averaged overall profile for landfalling tornadic hurricanes. In the latter case, the effects of hurricane translation are effectively removed by the averaging process, so that the resulting profile approximates one that may be obtained around a stationary, symmetric hurricane. The average of the quadrants forms a standard against which each of the quadrant profiles can be compared.

The differences between the temperature profiles (not shown) are relatively small. However, in the lower troposphere the rear quadrants are significantly warmer than the front quadrants. In addition, the right quadrants are slightly warmer than the left quadrants in the middle and upper troposphere; the differences are most significant at upper levels. These temperature differences, along with enhanced moisture in the front quadrants, combine to suggest considerable quadrant-to-quadrant variation in thermodynamic instability. In particular, the variations in low-level temperature and

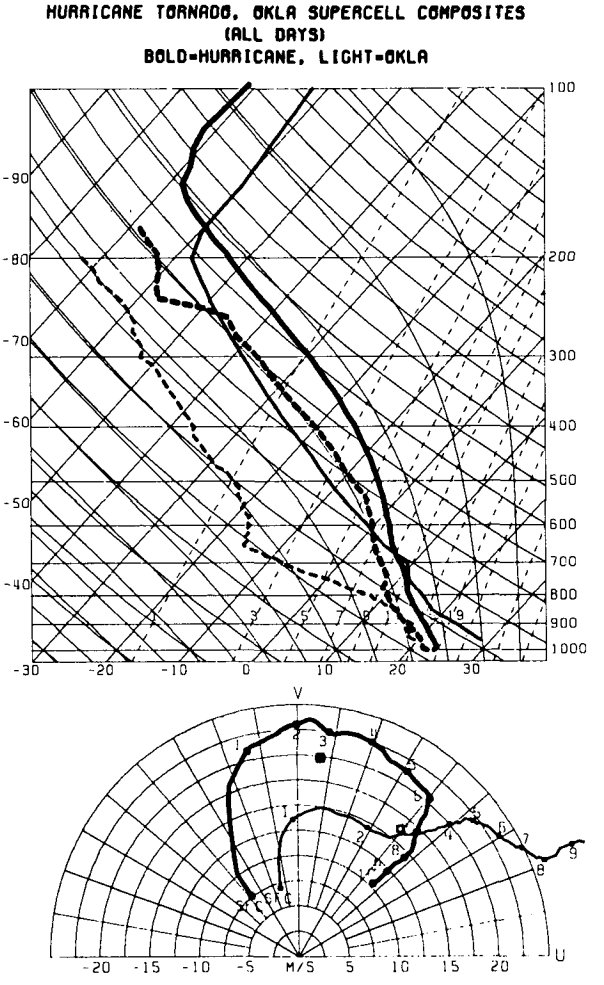

FIG. 9. Skew T–log p and hodograph diagrams for the hurricane tornado close-proximity composite (heavy lineweight) and Oklahoma supercell composite of Bluestein and Jain (light lineweight). The U and V components of the Oklahoma composite are relative to true zonal and meridional directions. Boxes mark 0–6 km mean winds.

TABLE 3. Mean parameters of tornado proximity soundings data stratified by proximity.

Variable	General proximity	Close proximity
Number of temperature profiles	180	10
Number of wind profiles	169	10
Range from center	329.3	264.8
CAPE (J kg^{-1})	760.4	253.4
BRN shear (m s^{-1})	9.8	14.0
Bulk Richardson number	66.3	3.3
0–3 km H_r	0.28	0.52
0–6 km H_r	0.22	0.42
0–12 km H_r	0.15	0.39
0–3 km H_t (m s^{-2})	0.035	0.078
0–6 km H_t (m s^{-2})	0.023	0.055
0–12 km H_t (m s^{-2})	0.016	0.046
0–3 km ω_s (s^{-1})	0.0037	0.0068
0–6 km ω_s (s^{-1})	0.0025	0.0051
0–12 km ω_s (s^{-1})	0.0017	0.0040

moisture are consistent with the patterns of variation of CAPE seen in Fig. 2.

The differences between the hodographs are even more striking than those between the thermal properties of the quadrants. To highlight these differences, Fig. 12 shows the four hodographs drawn at the centers of their respective quadrants relative to the mean hurricane center, with each hodograph rotated appropriately to reflect the systematic changes in orientation of the local (U, V) coordinates. The mean of the four quadrants, which serves as a reference, is also shown.

It is evident from the figure that the hodograph in the left-rear (LR) quadrant tends to fold back on itself as winds first veer, then back, with height. This is quite different from what occurs in the right-front (RF) quadrant, where winds veer continuously with height. In general, the RF hodograph shows particularly large amplitudes of windspeed and shear and a more "open" shape than the other quadrants. The comparison between quadrants suggests that the four hodographs would become nearly equal to the mean if:

1) a sheared mean flow from rear to front of the hurricane and varying in magnitude from 1.4 m s^{-1} at the surface to 7.6 m s^{-1} at 10 km altitude were removed from all quadrants. The shear in this component of flow is not uniform with height, but is concentrated somewhat at lower altitudes.

2) An additional across-hurricane mean flow from right to left, ranging from 1.4 m s^{-1} at the surface to roughly 2 m s^{-1} at 1 km altitude, were removed from the low-level winds. This component of flow becomes negligible above 4 km.

Thus, most of the systematic azimuthal variation in the hodographs can apparently be explained in terms of the superimposition of an almost unidirectionally sheared steering current on the circularly symmetric internal circulation of the hurricane itself.

To compare the wind profiles shown in Fig. 12, a t test was applied at each sigma level, under the assumption that the variances from each profile were not necessarily the same (see, e.g., Dixon and Massey 1969, p. 119). Application of this technique to all possible combinations of hodographs from the four quadrants confirms that the differences between the wind profiles are highly significant statistically, often at better than the 1% level, especially in the middle and upper troposphere.

A summary of key sounding parameters for the four quadrants is given in Table 4. The table shows that the mean distance from raob site to hurricane center ranges from 256 to 421 km in the various quadrants. However, most of the raobs were made sufficiently far from the hurricane centers that the patterns in the composites and their characteristic parameters would not change greatly if the data used in the compositing were more carefully controlled with respect to range.

As Table 4 indicates, the mean CAPEs vary considerably in the four quadrants, with a minimum of 300 J kg^{-1} in the left-front (LF) quadrant and a maximum of 1212 J kg^{-1} in the LR. Mean CAPE in the right-rear (RR) quadrant is 1031 J kg^{-1}, while that in the RF quadrant is 684 J kg^{-1}. All these values are considerably smaller than the mean CAPE of the Great Plains tornado environment discussed in subsection 3c. The mean LR CAPE is the most uncertain, owing to the relatively small sample size (21 raobs) in that

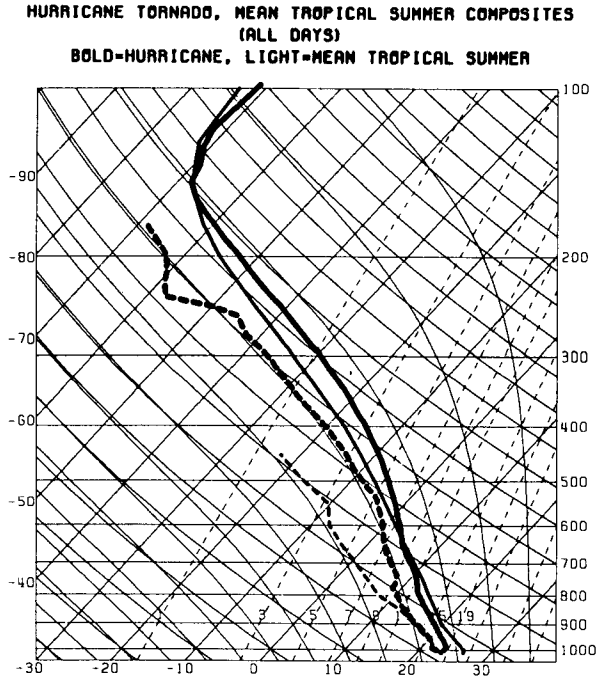

FIG. 10. Skew T-log p diagram showing the hurricane–tornado close-proximity composite sounding (heavy lineweight) and Jordan mean hurricane season sounding (light lineweight).

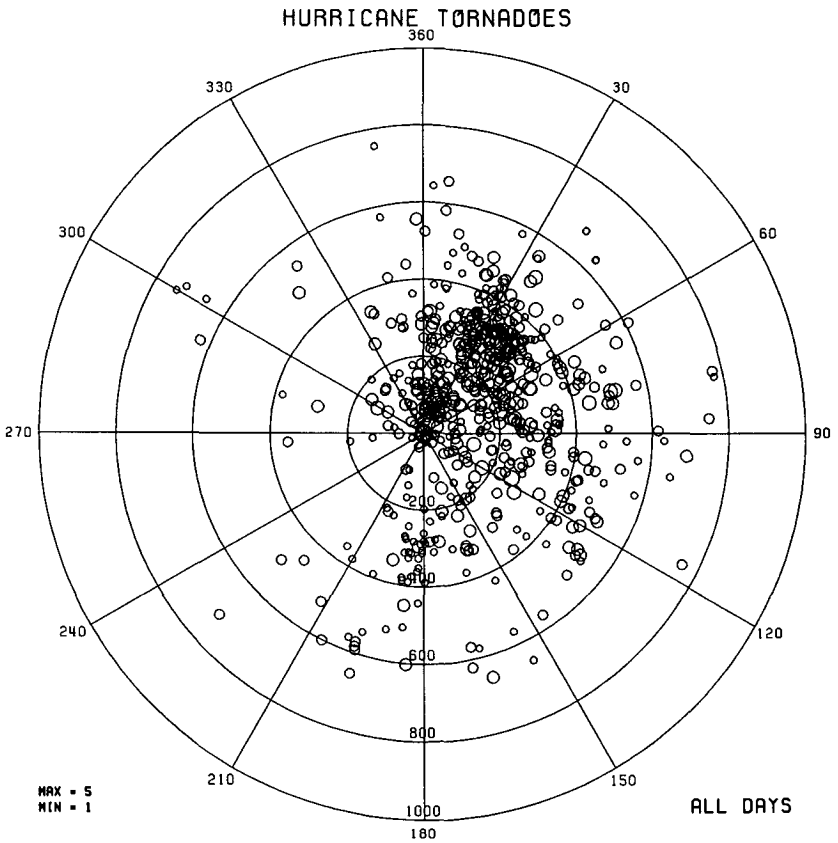

FIG. 11. Locations of all reported hurricane tornadoes, 1948–86. Format of diagram is as in Fig. 1a. Azimuths of tornado locations are defined relative to hurricane motion at tornado time. Areas of circles are proportional to unity plus the F-scale rating of the tornado. Note bimodal clustering of data points in right-front quadrant.

quadrant and the presence of several very unstable profiles there. Examination of mean values of θ_w in the lowest 500 m shows that the RR quadrant has the highest value, 23.2°C, while the LF quadrant has the lowest, 21.5°C. Surface and low-level relative humidities are distinctly higher in the RF quadrant, and the lifting condensation level (LCL) is at its lowest altitude (highest pressure) there.

The reduction of CAPE in the LF quadrant is consistent with the lowered surface temperatures analyzed by Novlan and Gray (1974) in tornado-producing hurricanes. Mechanisms that might be responsible for the cooler boundary layer in the LF quadrant include the adiabatic core cooling experienced by inflowing air parcels that have been separated from the warm sea surface for relatively long times (Novlan and Gray 1974), rain cooling of relatively dry air entrained into the hurricane circulation from the fringes of the storm (McCaul 1987), and the weak background baroclinicity that would be expected if sheared westerlies were influencing the hurricane.

The mean BRN shears varied from quadrant to quadrant in a pattern much different than that seen with CAPE. The mean shear is greatest, 11.3 m s^{-1}, in the RF quadrant, and least, 6.5 m s^{-1}, in the LR. Mean values of BRN range from 32.6 and 33.5 in the LF and RF quadrants to 119.0 and 190.7 in the RR and LR quadrants. The BRNs in the front quadrants are within the "possible supercell" range, according to Weisman and Klemp (1982, 1984). The means of each of the helicity parameters exhibit large quadrant-to-quadrant variations, with values in the RF quadrant being typically about four times larger than those in the LR quadrant. Mean 0–3 km H_r and H_t in the RF quadrant are 0.34 and 0.049 m s^{-2}, respectively.

e. Variations with range from hurricane center

In addition to the rather large azimuth dependence, hurricane-spawned tornadoes also display preferred locations with respect to range from the center of the parent hurricane. In Fig. 13 is shown the distribution of the ranges of all 626 hurricane tornadoes from their hurricane centers. There is a distinct peak in the 200–400 km interval, with a "shoulder" just inside approximately the 160-km range. When only tornadoes oc-

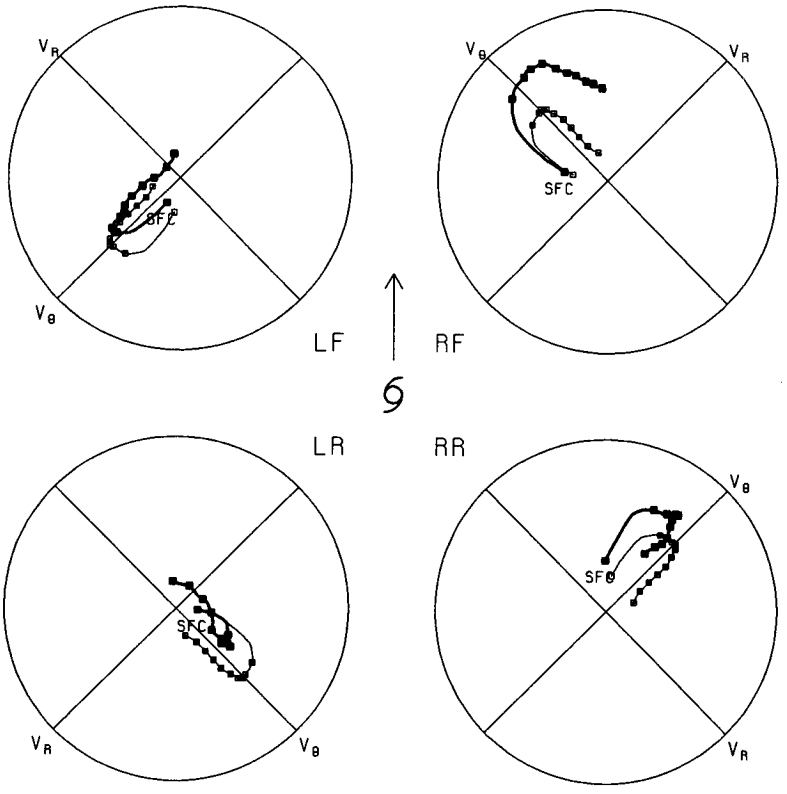

FIG. 12. Quadrant composite hodographs (heavy lines) arranged in their respective quadrants around the composite hurricane, which is assumed to be moving to top of diagram as shown. Mean hodograph of the four quadrants (light lines) is shown in each quadrant for reference. Boxes mark winds at each 1-km increment of altitude from the surface through 10 km. The labels V_r and V_θ indicate the radial and tangential components of wind, elsewhere referred to as U and V. The label "SFC" is plotted just below the surface wind box for the individual quadrant hodographs. Radii of hodograph circles correspond to a wind speed of 25 m s^{-1}.

curring on the "day of landfall" (i.e., within 12 h of the time of hurricane landfall) are plotted, the "shoulder" becomes a distinct separate peak (see also Fig. 13). Evidently, it is possible to classify hurricane tornadoes into two regimes, "outer rainband" and "core." The first class includes tornadoes that occur at large range, especially 200–400 km from the hurricane centers; these tornadoes may be associated with features such as the "stationary band complex" (Willoughby et al. 1984). Core tornadoes are those that occur in the inner rainbands and, occasionally, the eyewall of the hurricane; they tend to occur mainly on the day of landfall in strong, well-organized hurricanes. Only 19% of the documented tornadoes in this study can be categorized as being the core type. Others have also found evidence of the existence of this core tornado mode (Gentry 1983; Weiss 1987,,Fig. 8b). This bimodal distribution of hurricane tornadoes may also be observed in the azimuth–range plot given earlier in Fig. 11. Both core and outer rainband tornadoes occur most often in the RF quadrant.

The reason for the presence of the two modes of tornadoes might be discovered by compositing the available landfall day raob data with respect to range. Unfortunately, the few tornado proximity raobs that lie within 160 km of hurricane centers were generally made either in weak hurricanes or well after hurricane landfall, and thus do not describe the core tornado environment well. Only four complete tornado proximity raobs were available that might address the problem, but these did not appear to come from a representative sample of hurricane core environments. In general, the raobs considered here are suitable for studying only the environments of the outer rainband type of hurricane tornadoes.

To get some idea of how the tornado environments differed with range from the hurricane centers, general proximity composites were made of all available raobs in the RF quadrant from 12 h prior to hurricane landfall to 60 h after landfall at ranges less than 300 km ("inside the outer rainband") and more than 300 km ("outside the outer rainband") from the hurricane center. The mean radius of the "inside" raobs from their respective hurricane centers was 205 km, while

TABLE 4. Mean parameters of tornado proximity soundings data stratified by quadrant.

Variable	LF	RF	RR	LR
Number of temperature profiles	36	86	44	21
Number of wind profiles	32	81	42	20
Range from center	255.9	330.6	421.1	314.6
CAPE (J kg^{-1})	299.8	684.2	1031.4	1212.3
BRN shear (m s^{-1})	8.4	11.3	8.9	6.5
Bulk Richardson number	32.6	33.5	119.0	190.7
0–3 km H_r	0.30	0.34	0.23	0.07
0–6 km H_r	0.19	0.29	0.18	0.06
0–12 km H_r	0.10	0.21	0.14	0.02
0–3 km H_t (m s^{-2})	0.031	0.049	0.022	0.012
0–6 km H_t (m s^{-2})	0.019	0.033	0.013	0.009
0–12 km H_t (m s^{-2})	0.011	0.023	0.010	0.002
0–3 km ω_s (s^{-1})	0.0036	0.0048	0.0027	0.0008
0–6 km ω_s (s^{-1})	0.0023	0.0034	0.0018	0.0006
0–12 km ω_s (s^{-1})	0.0014	0.0023	0.0013	0.0004

that for the "outside" raobs was 407 km. Because of the scatter of raob positions and the variability of range of the outer rainbands from hurricane to hurricane, this composite cannot be expected to resolve the details of changes in the mesoscale meteorological fields across specific rainbands (see, e.g., Barnes et al. 1983, or Powell 1990). Nevertheless, it can reveal something about the general differences between the fields near and far away from the hurricane centers.

The results are shown in Fig. 14. As expected, the tangential winds "inside" the outer rainband are considerably stronger than those "outside." The t test shows the differences are highly significant throughout the troposphere. In addition, the t test shows that the radial winds "outside" are significantly stronger than those "inside" above 8.6 km (340 hPa) in the upper-level outflow layer. Dewpoints are significantly higher below 650 hPa (3.6 km) "inside" the outer rainband as compared to "outside." Temperatures "inside" are significantly higher in the layer 590–280 hPa (4.5–10 km). It must be kept in mind that these composites are created using only "tornado proximal" raob data and are thus probably somewhat biased toward more intense conditions, regardless of range from the hurricane center.

Table 5 summarizes the characteristics of the raobs in the two range categories. Because the warmer temperatures aloft in the "inner" raobs are counterbalanced by enhanced low-level moisture, the mean CAPEs in the two categories show no significant differences. Shears and helicities are slightly larger for the "inside" raobs, but values are high in both range intervals. BRNs are larger for the "inside" raobs, but when ac-

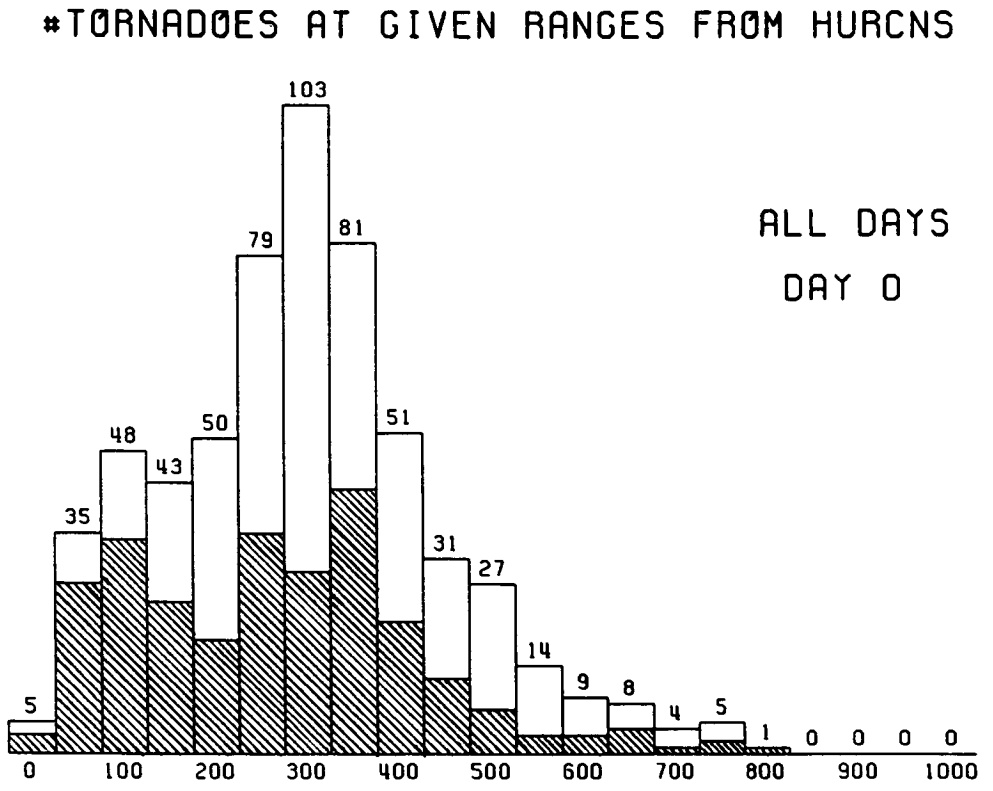

FIG. 13. Range distribution of reported hurricane tornadoes during 1948–86, for all days relative to landfall (total bar height), with tornadoes on landfall day itself indicated by hatching. Range bins are 50 km wide and are centered on the labeled values. Note distinct peak near 100-km range for landfall-day tornadoes.

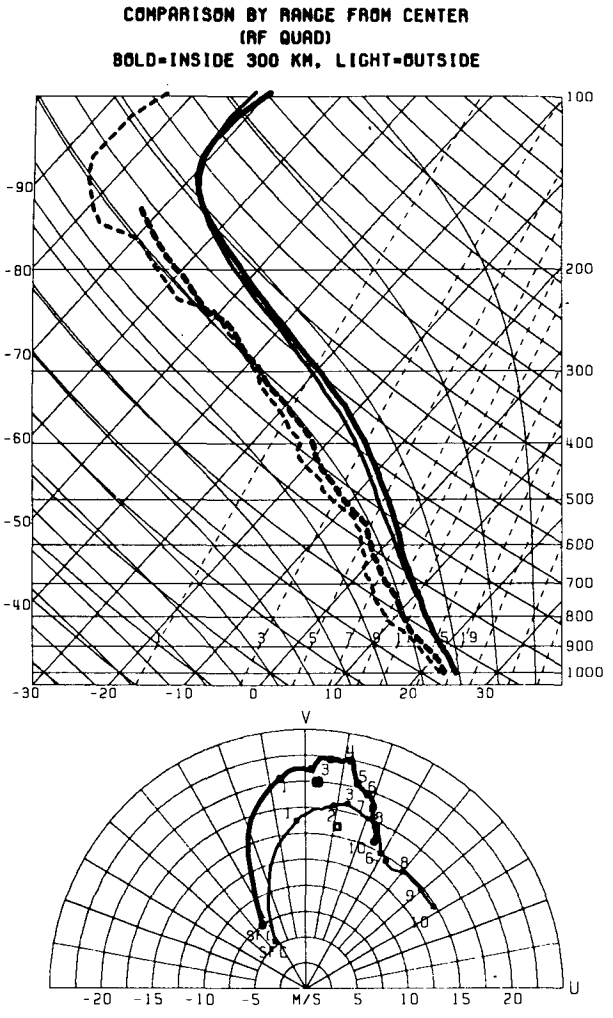

FIG. 14. Skew T–log p and hodograph diagrams for composite RF quadrant soundings from "inside" (heavy lines) and "outside" (light lines) 300-km range from the hurricane centers. Format is as in Fig. 8.

count is taken of the inherent variability of BRN, the difference is not significant.

f. Variations with respect to time after landfall

Most hurricane tornadoes tend to occur near the time of hurricane landfall. This fact, illustrated in Fig. 15, is in agreement with findings of previous investigators (Novlan and Gray 1974; Gentry 1983; Weiss 1987). However, Fig. 15 also shows that significant tornado activity may persist through at least two days following landfall. This persistent tornado activity is somewhat puzzling, especially in view of the tendency of hurricanes to dissipate rapidly after making landfall.

To examine how the circulations of tornadic hurricanes change after they move inland, the raobs were stratified with respect to time after landfall, yielding composite profiles for successive 24-h periods (days) centered on landfall time. The composite consisting of the average of all raobs taken within 12 h of landfall time is called "landfall day" or "day 0." The day 1 composite represents the average of all raobs taken between 12 and 36 h after hurricane landfall. Other "days" are defined in an analogous fashion. Only composites for the RF quadrant of the hurricanes are given here, owing to insufficient data in the other quadrants when stratified by time after landfall. Soundings taken farther than 400 km from the centers of hurricanes were excluded from the day 0 composite to ensure that the mean range of the raobs used would be comparable to those on days 1 and 2.

In Fig. 16 are shown the composite RF quadrant profiles from day 0 and day 2 after landfall. The day 1 composite lay generally between those of days 0 and 2 and is not shown. Although the number of raobs used in making the composites was small (31 raobs for day 0; 7 raobs for day 2), the differences between the winds aloft are significant and are believed to be representative. The tangential components on day 2 are significantly weaker, according to the t test, near the surface and at most layers above 9.3 km (315 hPa). According to the same test, the outward-directed radial components on day 2 are significantly stronger between 5.2–8.5 km (540–350 hPa). Temperature and dewpoint profiles do not differ significantly.

The key aspects of the hodograph changes shown in Fig. 16 are that the winds in the lowest 1 km weaken with time, while those above about 4 km maintain strength and veer with time. This tendency is necessarily accompanied by an increase in mid- and upper-level vertical shear, graphically illustrated by the growth of hodograph arc length with time. These changes in the winds aloft lead to modification of the mean winds in the convection-bearing layer and to increases in storm cell-relative winds through much of the middle and upper troposphere. The net effect of the hodograph changes is to help sustain or even cause increases in

TABLE 5. Mean parameters of tornado proximity soundings data stratified by range from hurricane center.

Variable	$R \leq 300$	$R > 300$
Number of temperature profiles	36	27
Number of wind profiles	34	26
Range from center	204.9	407.3
CAPE (J kg^{-1})	670.0	703.9
BRN shear (m s^{-1})	11.8	10.5
Bulk Richardson number	47.5	21.2
0–3 km H_r	0.37	0.34
0–6 km H_r	0.30	0.30
0–12 km H_r	0.23	0.23
0–3 km H_t (m s^{-2})	0.049	0.039
0–6 km H_t (m s^{-2})	0.033	0.027
0–12 km H_t (m s^{-2})	0.024	0.020
0–3 km ω_s (s^{-1})	0.0050	0.0043
0–6 km ω_s (s^{-1})	0.0035	0.0032
0–12 km ω_s (s^{-1})	0.0025	0.0022

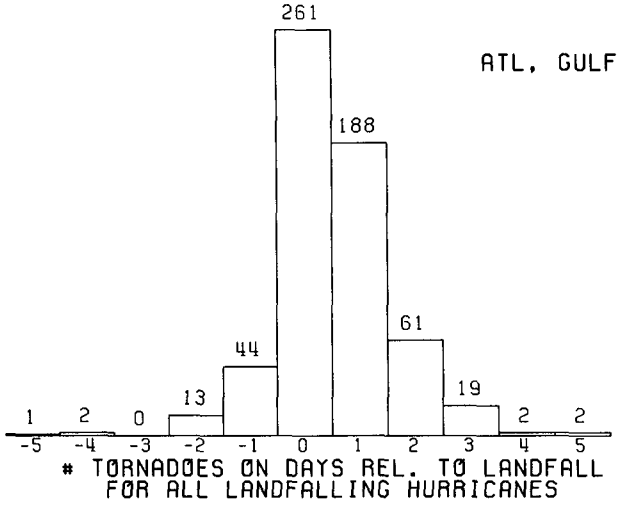

FIG. 15. Temporal distribution of reported hurricane tornadoes, 1948–86, relative to day of landfall (day 0 = within 12 h of landfall; day 1 = from 12 to 36 h after landfall, etc.).

the values of H_l in the dying hurricanes, sometimes for as long as three days after landfall.

Table 6 gives the key values of raob parameters for the day 0–2 stratifications of the data. The mean of the CAPEs shows a decrease on day 2. Figure 16 shows that this reduction in CAPE is due to warmer temperatures near 600 hPa on day 2. However, in view of the size of the rms variations and the smallness of the sample of day 2 data, these temperature and CAPE differences cannot be considered significant. The shear and helicity parameters, as suggested earlier, tend to increase with time after landfall.

Although the data given in Fig. 16 are believed to be representative, further evidence is desirable, especially in view of the fact that not all the hurricanes sampled on day 2 are also sampled on day 0. It is important to demonstrate that individual hurricanes also display this persistence of strong circulation aloft through several days following landfall. Hurricane Danny (1985) serves as a good example in this regard, because four separate raobs were taken in this storm's RF quadrant at ranges in the interval 230–320 km, during the time interval 8–56 h following landfall. Inspection of the hodographs (not shown) confirms that windspeeds of 20–25 m s^{-1} are consistently maintained in the midtroposphere through the period and that, in spite of decreases in shear in the lowest 1 km, shears aloft (i.e., hodograph arc lengths) tend to increase with time. The same general evolution of winds and shears has been found in four other hurricanes for which at least two days of tornadic raobs were available after landfall.

g. *Variations with respect to time of day*

Other investigators have noted diurnal variations in occurrence times of hurricane tornadoes (Fujita et al. 1972; Weiss 1987). The diurnal distribution of tornado events in the present data is shown in Fig. 17. Times are expressed in terms of local solar time, which is the equivalent of the local mean time of Kelly et al. (1978). The distribution features a distinct maximum in early and midafternoon, slightly earlier than that found by Kelly et al. for all United States tornadoes. This finding suggests that solar radiational heating might be important even in the mostly cloudy environments characteristic of landfalling hurricanes. Alternatively, there could be a diurnal observational bias. These two possibilities were also considered by Weiss (1987).

To see how the mean environmental conditions varied during the day, the raobs were stratified by time of day and composited. Because of the importance of azimuthal variations in the data and of the preponderance of data in the RF quadrant, the composites were restricted to the RF quadrant on days 0–2 (combined) relative to landfall. Sufficient data were available

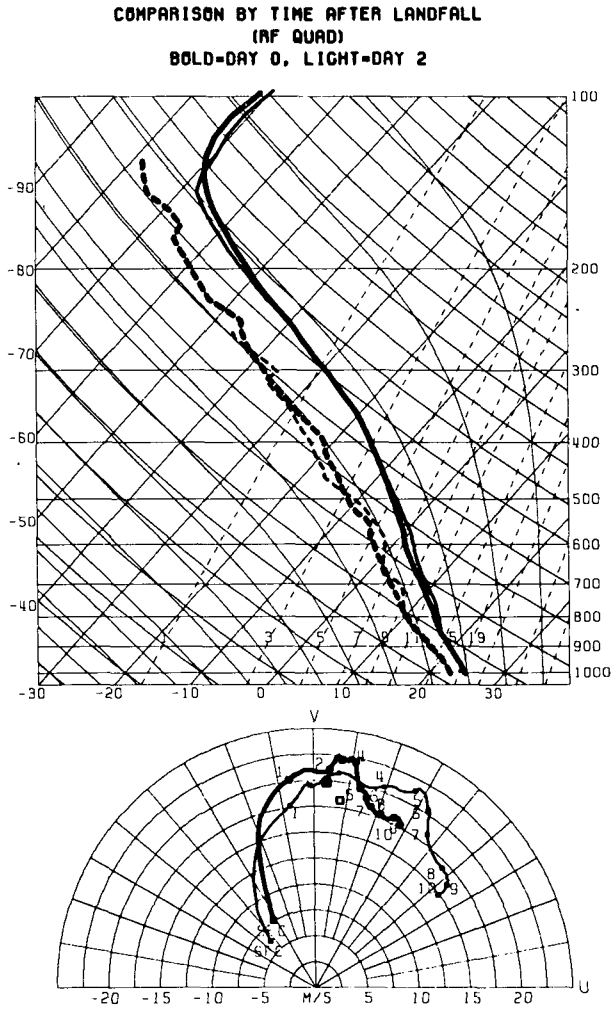

FIG. 16. Skew T–log p and hodograph diagrams for composite RF quadrant soundings from day 0 (heavy lines) and day 2 (light lines), relative to landfall. Format is as in Fig. 8.

TABLE 6. Mean parameters of tornado proximity soundings data stratified by time (days) after landfall.

Variable	Day 0	Day 1	Day 2
Number of temperature profiles	31	17	7
Number of wind profiles	29	16	7
Range from center	241.3	267.7	255.1
CAPE (J kg^{-1})	672.9	685.5	258.3
BRN shear (m s^{-1})	11.7	11.3	13.6
Bulk Richardson number	51.0	19.8	3.1
0–3 km H_r	0.30	0.40	0.45
0–6 km H_r	0.24	0.35	0.39
0–12 km H_r	0.19	0.25	0.33
0–3 km H_t (m s^{-2})	0.045	0.051	0.056
0–6 km H_t (m s^{-2})	0.030	0.035	0.037
0–12 km H_t (m s^{-2})	0.020	0.025	0.033
0–3 km ω_s (s^{-1})	0.0044	0.0054	0.0056
0–6 km ω_s (s^{-1})	0.0032	0.0039	0.0040
0–12 km ω_s (s^{-1})	0.0021	0.0027	0.0032

to create only two composites, one representative of "morning" (1200 UTC) conditions, the other of "evening" (0000 UTC) conditions. These composites are shown in Fig. 18. The buoyancy and shear parameters of the morning and evening sounding data are given in Table 7.

As expected, the evening composite exhibits warmer surface temperatures than the morning composite. Interestingly, however, the evening composite was also warmer at nearly all levels. This result is consistent with that obtained by Sheets (1969) in his diurnal stratification of hurricane soundings. According to the t test, the differences are significant at the 5% level or better in several shallow layers below 850 hPa (1.5 km) and in a deeper layer aloft between 210–360 hPa (8.2–11.9 km). The evening CAPE, 700 J kg^{-1}, is only slightly larger than that of the morning composite, 646 J kg^{-1}. In view of the variability of CAPE, these differences are not statistically significant at the 5% level. In fact, the dewpoints of the evening composite are generally slightly higher than the morning's, but only at middle and upper levels, where they do not strongly influence CAPE. The winds do not display significant differences at any level. All these conclusions are confirmed by inspecting the trends in parameters given in Table 7.

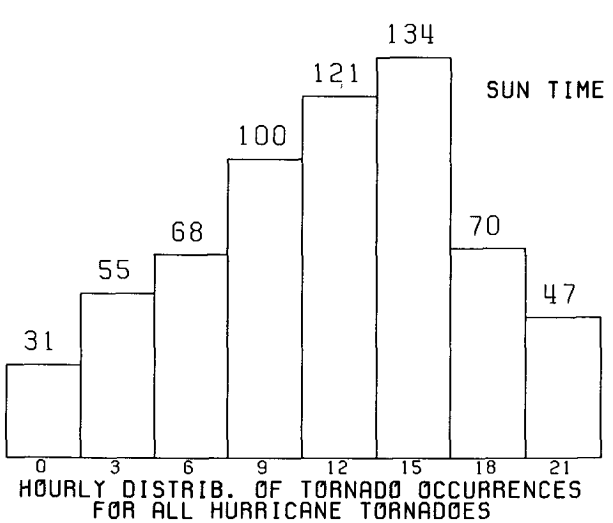

FIG. 17. Hourly distribution of reported hurricane tornadoes, 1948–86, with respect to local solar time. Time bins are 3 h wide and are labeled with the first hour within the bin; i.e., bin labeled "12" contains all tornadoes occuring between 1200 and 1459 LST.

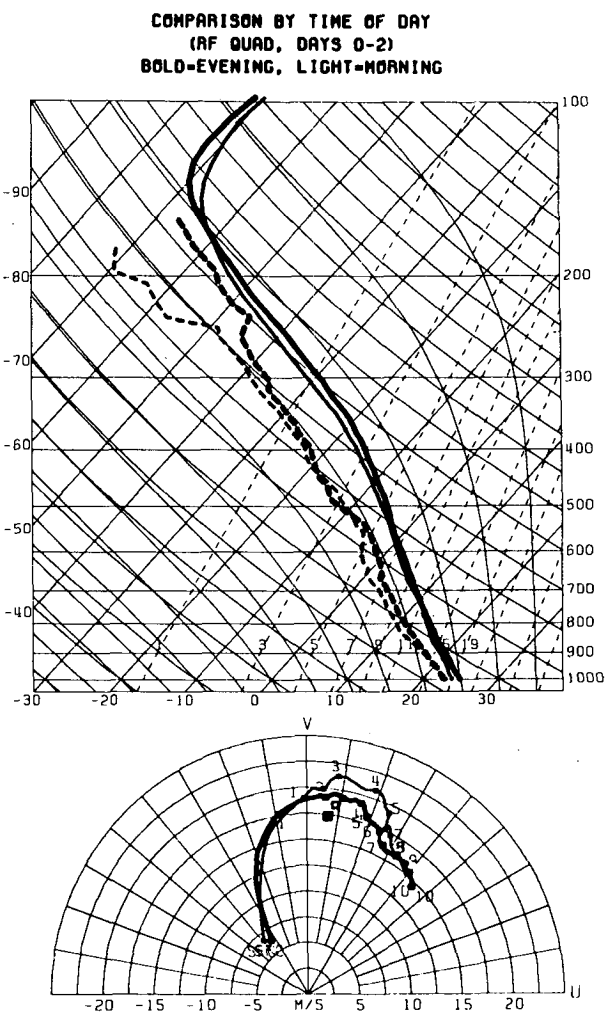

FIG. 18. Skew T-log p and hodograph diagrams for composite "morning" (0800–1200 UTC) and "evening" (2000–0000 UTC) soundings in the RF quadrant. Format is as in Fig. 8.

The lack of difference in CAPE between the morning and evening composites suggests that the diurnal variation of hurricane tornado activity might be the result of an observational bias. However, Fig. 17 shows that the two raob times studied correspond to times when tornado production rates are roughly equal; raobs taken at approximately 0800 UTC and 2000 UTC would be needed to study the diurnal changes in a definitive way. It appears likely that the possible buoyancy increases thought to be responsible for the afternoon peak in

TABLE 7. Mean parameters of tornado proximity soundings data stratified by time of day.

Variable	Morning (0800–1200 UTC)	Evening (2200–0000 UTC)
Number of temperature profiles	19	26
Number of wind profiles	19	26
Range from center	281.4	306.1
CAPE (J kg^{-1})	646.3	699.8
BRN shear (m s^{-1})	12.3	11.4
Bulk Richardson number	20.2	57.2
0–3 km H_r	0.37	0.39
0–6 km H_r	0.34	0.29
0–12 km H_r	0.26	0.23
0–3 km H_t (m s^{-2})	0.044	0.051
0–6 km H_t (m s^{-2})	0.030	0.034
0–12 km H_t (m s^{-2})	0.022	0.026
0–3 km ω_s (s^{-1})	0.0046	0.0052
0–6 km ω_s (s^{-1})	0.0035	0.0036
0–12 km ω_s (s^{-1})	0.0024	0.0025

tornadic storms are simply not adequately sampled by the present data.

h. Variations with respect to hurricane forward speed

Weiss (1985) found that the forward translational speed of hurricanes was positively correlated with tornado productivity. Results presented in subsection 3d suggest that shear in the hurricane steering current can influence the generation of conditions favorable to genesis of tornadic storms. It seems possible that more strongly sheared steering currents might also have stronger mean flow speeds and that hurricanes influenced by such currents would exhibit faster translational speeds. To study this, composite profiles in fast and slow moving hurricanes were constructed.

To establish which hurricanes should qualify as "fast" and "slow" moving, the number distribution of hurricane translational speeds was examined. The hurricane translational speeds were estimated by finite differencing of hurricane positions; one estimate of hurricane speed was recorded for each 6-h hurricane position report in the HURDAT data on days 0–2 relative to landfall, for both tornadic and nontornadic hurricane landfalls.

The distributions of the translational speeds for both tornadic and nontornadic landfalls are shown in Figs. 19a–b. The peak of the distribution for the tornadic subset lies in the 6 (i.e., 5–7) m s^{-1} bin, while for the nontornadic subset the 4 (i.e., 3–5) m s^{-1} bin is favored. This suggests that the tornadic hurricanes are indeed characterized by faster translational speeds. However, closer inspection of the figures reveals that this conclusion breaks down when speeds greater than approximately 15 m s^{-1} are considered. For such very fast translational speeds, nontornadic events tend to predominate. This pattern is reflected in the mean translation speeds of the two distributions: 6.85 m s^{-1} for the tornadic landfall data but 7.42 m s^{-1} for the nontornadic data. These speeds are somewhat faster than those reported by Weiss (1985). In any case, inspection of Fig. 19a suggests that adequate raob data samples will be obtained if hurricanes with forward speeds less than 4 m s^{-1} are defined as "slow," while those with forward speeds not less than 8 m s^{-1} are defined as "fast."

The composite profiles for the RF quadrants of these slow and fast moving hurricanes are shown in Fig. 20. It is clear from the figure that the winds aloft are considerably stronger for the fast hurricanes than for the slow ones. In fact, at an altitude of 10 km, the winds

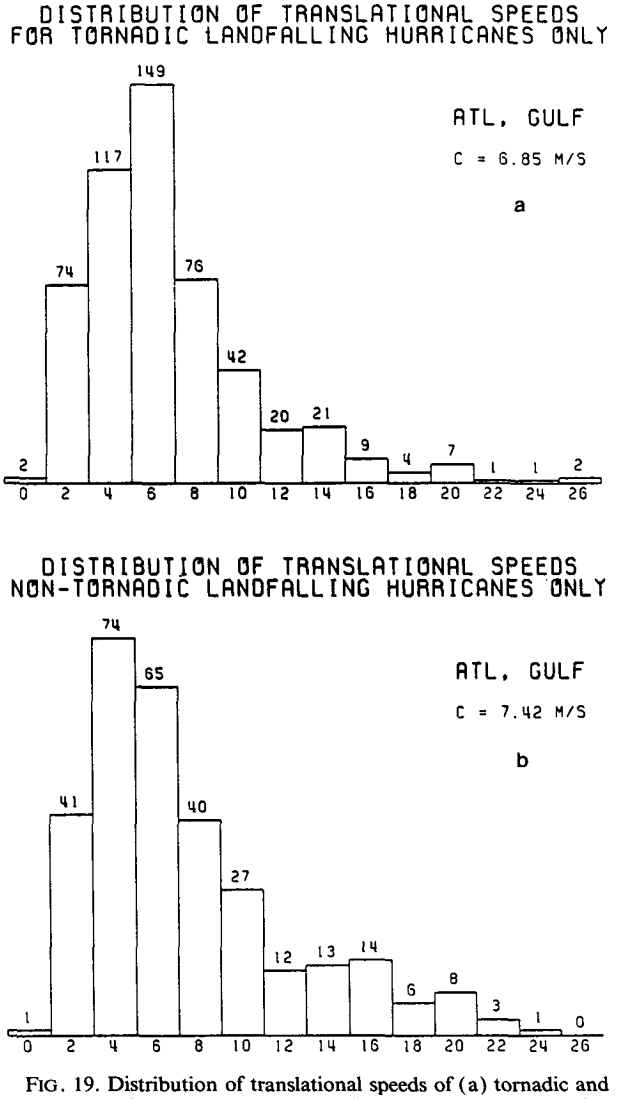

FIG. 19. Distribution of translational speeds of (a) tornadic and (b) nontornadic hurricanes based on estimates made every 6 h during days 0–2 relative to landfall. Speed bins, each of width 2 m s^{-1}, are labeled with value corresponding to midpoint of bin; i.e., 8 m s^{-1} bin encompasses all speeds between 7–9 m s^{-1}.

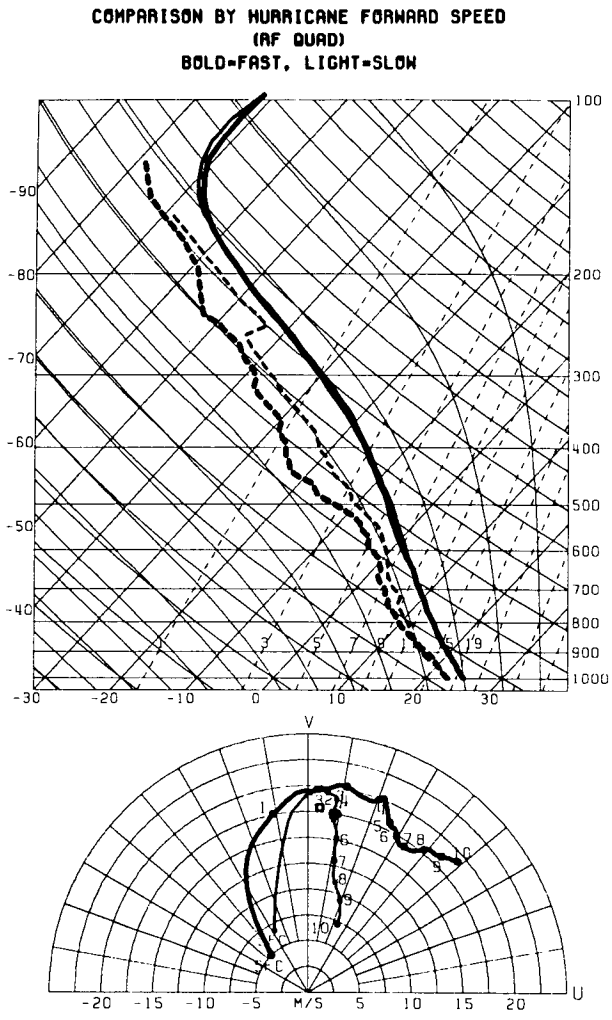

FIG. 20. Skew T–log p and hodograph diagrams for RF quadrant composites on days 0–2 (inclusive) for "fast-moving" (heavy lines) and "slow-moving" (light lines) tornadic hurricanes. Format is as in Fig. 8.

for the fast hurricanes are approximately 13 m s^{-1} stronger. The peak rms variability of the tropospheric wind components is on the order of 5–9 m s^{-1} in both profiles, considerably smaller than the reference values for the entire set of general proximity raobs. As a result, the wind differences are judged to be statistically significant, often at better than the 1% level, everywhere above 3.5 km (650 hPa). The dewpoints of the fast hurricanes were significantly drier than those of the slow hurricanes in much of the layer from 740–370 hPa (2.7–8.1) km. The temperature profiles of the two composites did not differ significantly from one another.

Table 8 gives the summary of raob parameters for the tornadic soundings from these fast and slow-moving hurricanes. Differences in CAPE are negligible, but the fast-moving hurricanes display much larger mean values of shear and helicity.

TABLE 8. Mean parameters of tornado proximity soundings data stratified by hurricane forward speed.

Variable	$c < 4$ m s^{-1}	$c > 8$ m s^{-1}
Number of temperature profiles	12	18
Number of wind profiles	12	17
Range from center	268.0	341.2
CAPE (J kg^{-1})	763.7	699.4
BRN shear (m s^{-1})	9.9	12.8
Bulk Richardson number	99.4	18.9
0–3 km H_r	0.21	0.46
0–6 km H_r	0.23	0.37
0–12 km H_r	0.21	0.28
0–3 km H_t (m s^{-2})	0.022	0.072
0–6 km H_t (m s^{-2})	0.017	0.047
0–12 km H_t (m s^{-2})	0.014	0.035
0–3 km ω_s (s^{-1})	0.0031	0.0066
0–6 km ω_s (s^{-1})	0.0026	0.0046
0–12 km ω_s (s^{-1})	0.0019	0.0032

The present database contained very few raobs made in hurricanes traveling at speeds in excess of 15 m s^{-1}. Thus the "fast" composite shown in Fig. 20 describes the characteristics of hurricanes having translation speeds mainly in the 8–15 m s^{-1} range. The raob data are at present insufficient to study the characteristics of hurricanes that move faster than 15 m s^{-1}, and thus the questions about why such very fast-moving hurricanes tend to lose their tornadic potential cannot yet be answered.

i. Variations with hurricane intensity and size

Novlan and Gray (1974), Gentry (1983), and Weiss (1985) have all pointed out that the likelihood of hurricane-tornado activity increases with the "intensity," i.e., peak sustained surface winds, of the landfalling hurricane. The present data support this notion, but also suggest that hurricane "size" (Merrill 1983) is important. Hurricanes notable for both their size and intensity have been among the most prolific tornado producers in the database: Audrey (1957), Carla (1961), Beulah (1967), and Allen (1980). In Table 9 are presented estimates of mean intensity and size for those landfalling hurricanes producing either 0, 1, or more than 8 tornadoes in the United States during the

TABLE 9. Mean intensity and size estimates of NT = 0, NT = 1, and NT > 8 hurricanes.

Class	NL	MAXWND	ROCI	Area
NT = 0	24	21.9	1.40	8.28
NT = 1	7	28.7	1.88	12.77
NT > 8	19	47.1	2.93	32.53

NL = number of separate landfalls.
MAXWND = mean intensity at landfall (m s^{-1}).
ROCI = mean radius of outer closed isobar (at surface, deg lat).
Area = mean area within ROCI (square deg lat).

period 1964–86. Hurricane intensity estimates at landfall were derived from the HURDAT tape data, while size estimates were obtained in the form of estimates of the radius of outer closed isobar (ROCI) from subjective analysis of synoptic weather map data. For the hurricanes producing no tornadoes, events prior to 1964 were excluded owing to the lack of adequately detailed weather maps. The map analyses were drawn to a resolution of 4 hPa, and are thus only capable of giving rather crude estimates of ROCI. Finer-scale analyses using more complete surface data would undoubtedly yield larger and more precise ROCI estimates, but such a study is beyond the scope of this paper.

The means listed in Table 9 indicate that the hurricanes that produced major tornado outbreaks had average peak winds of 47.1 m s^{-1} at landfall, compared to a mere 21.9 m s^{-1} for the nontornadic hurricanes. The major tornado outbreak producers also had average ROCIs of 2.93° latitude, more than twice that of the 1.40° for nontornadic hurricanes. These ROCIs are smaller than those described by Merrill (1983), probably because of differences in the hurricanes sampled and, especially, in the resolution of pressure contour analyses used in measuring ROCI. The size and intensity of those hurricanes that produced only one tornado resemble those of the nontornadic hurricanes more than they do the major outbreak producers.

While some of the hurricanes responsible for major tornado outbreaks were not particularly intense, they all had ROCIs larger than the mean of the nontornadic class of hurricanes. It appears that the area exposed to favorable hurricane-induced wind profiles is an important factor influencing overall tornado productivity. It is possible that the "strength" parameter described by Merrill (1983) could also be well-correlated with tornado productivity. Unfortunately, the strength parameter is very difficult to measure, and no data are available at present with which to test its importance.

In most hurricanes, the peak winds are confined to the inner core area, near the eyewall. Thus, to create a composite sounding that would accurately reflect the differences between intense and weak hurricanes, heavy reliance would have to be placed on raobs from the inner cores of the hurricanes. As pointed out in section 3e, the present database contains insufficient raob data from hurricane core regions to allow for a meaningful stratification of the data by intensity.

j. Variations with respect to landfall basin

Gentry (1983) and Weiss (1985) have described the dependence of tornado productivity on position of hurricane landfall point. The thrust of their observations was that hurricanes making landfall south of the latitude of the Carolinas were much more likely to spawn tornadoes than those making landfall farther north. Close examination of all the data suggests that the distinction can be simplified even more by asking in which coastal basin, Atlantic or Gulf of Mexico, the landfall took place. In terms of proportion of hurricanes that produce tornadoes, landfalls along the Florida east coast are virtually indistinguishable from those that strike the Atlantic coast farther north. Based on the NSSFC tornado data, it appears that landfalls occurring along the Atlantic coast are much less likely to spawn tornadoes than those along the Gulf.

Table 10 gives some statistics on the differences between Atlantic and Gulf landfalls relevant to hurricane tornado productivity. Gulf landfalls produce tornadoes 70% of the time, while Atlantic landfalls do so only 40% of the time. If data prior to 1964 are excluded, the proportion of tornadic landfalls increases to 88% in the Gulf basin but changes little in the Atlantic coast basin. Gulf landfalls produce, on average, 5.6 tornadoes apiece, while those on the Atlantic coast produce only 1.6. Even if only those hurricanes that actually produce tornadoes are considered, the Gulf landfalls are still more prolific, with 7.9 tornadoes apiece, compared to 4.0 apiece on the Atlantic coast. These facts lead naturally to questions about whether the characteristics of Gulf landfalling hurricanes differ in any important way from those of Atlantic storms.

To investigate this issue, composites of the raobs in the RF quadrants of landfalling Gulf and Atlantic hurricanes on days 0–2 relative to landfall were generated. The results, (not shown) indicate only a small surplus of CAPE in the Gulf hurricanes. However, *t* tests imply that the differences are not statistically significant. Thus, there is nothing to suggest that the tornadic Atlantic hurricanes have grossly different thermal or wind profile characteristics than the Gulf storms. This is confirmed by inspection of Table 11, which gives a summary of the raob parameters for the Atlantic and Gulf basin data. The basin-dependent differences in tornado productivity are probably ascribable to other factors.

There are at least three possible explanations for the differences in Atlantic and Gulf hurricane-tornado productivity. The first has to do with differences in mean intensity at landfall, the second with differences in tendency to weaken prior to landfall, and the third with differences in areal and temporal extent of land exposure of the RF quadrant following landfall.

TABLE 10. Tornado productivity of Atlantic and Gulf landfalls.

	Atlantic	Gulf
Number of landfalls	60	93
Number of tornadic landfalls	24	66
Number of nontornadic landfalls	36	27
Number of tornadoes	96	521
Number of tornadoes/landfall	1.60	5.60
Number of tornadoes/tornadic landfall	4.00	7.89

TABLE 11. Mean parameters of tornado proximity soundings data stratified by hurricane landfall basin.

Variable	Atlantic	Gulf
Number of temperature profiles	10	46
Number of wind profiles	9	44
Range from center	222.2	265.3
CAPE (J kg^{-1})	453.6	658.9
BRN shear (m s^{-1})	10.7	12.0
Bulk Richardson number	20.5	37.6
0–3 km H_r	0.36	0.36
0–6 km H_r	0.27	0.31
0–12 km H_r	0.24	0.23
0–3 km H_t (m s^{-2})	0.043	0.049
0–6 km H_t (m s^{-2})	0.031	0.032
0–12 km H_t (m s^{-2})	0.026	0.023
0–3 km ω_s (s^{-1})	0.0046	0.0050
0–6 km ω_s (s^{-1})	0.0032	0.0036
0–12 km ω_s (s^{-1})	0.0024	0.0024

Table 12 gives a summary of prelandfall intensity and intensity tendencies for landfalls occurring in the Atlantic and Gulf basins. According to the table, the mean landfall intensity for Gulf hurricanes is nearly 3 m s^{-1} greater than that for Atlantic storms. This intensity difference is simply too small to have been reflected in the available raob data. Note also that Atlantic landfalls occurring north of Savannah, Georgia (SAV), are, if anything, slightly more intense than those occurring farther south. The table also shows that Atlantic hurricanes are about three times as likely to start losing intensity before making landfall as they are to start gaining it, whereas Gulf hurricanes exhibit prelandfall gains in intensity as often as losses. In both basins, there is a superimposed bias toward prelandfall gains in intensity for tornadic hurricanes and a bias toward prelandfall losses in intensity for nontornadic hurricanes. Other hurricane-tornado investigators (Novlan and Gray 1974; Weiss 1985) have noted the tendency for tornadoes to be spawned preferentially by hurricanes that were gaining intensity at landfall time.

Another factor that probably reduces the tornado threat from landfalling Atlantic hurricanes is the fact that the Atlantic coast tends to parallel the mean hurricane track heading, so that most landfalls do not penetrate far inland. This tendency to "graze" the coast is described in Fig. 21, which gives the distribution of landfall incidence angles for both Atlantic and Gulf hurricanes. In tallying the data, direct, perpendicular coastline crossings are assigned a 90° incidence angle, while ones in which only the left quadrants are exposed to land are given a 0° angle. Figure 21 shows that the distribution of landfall incidence angle is roughly symmetrical about 90° for Gulf hurricanes, but is strongly skewed toward small angles for Atlantic storms. This suggests that the tornado-prone RF quadrant has relatively little exposure to land in the Atlantic coast basin. This is consistent with the findings of Gentry (1983).

4. Discussion

Because of the great differences between the composite Plains and hurricane-tornado environment profiles, one is prompted to ask what similarities they have that could be key to tornadic activity. With respect to the thermal profiles, the most fundamental similarity is that both composites are conditionally unstable, although to vastly different degrees. In the hurricane environments, buoyancy is small and reaches a maximum near 3–4 km altitude, whereas in the Great Plains the buoyancy is much larger and typically peaks near 10 km altitude.

The principal similarity in the winds is that both environments display strong, veering winds and shears, especially in the lower troposphere. The mean low-level shears in the hurricane environments are actually stronger than those found in typical Great Plains tornado environments. In the hurricanes, maximum winds are observed near 2–3 km altitude, while on the Great Plains the maximum occurs above 10 km. Thus, in both the hurricane and Great Plains tornado environments, the altitudes of maximum buoyancy and wind are well matched to each other. The implications of these relationships for convective storm strength are currently being investigated with numerical simulations.

Of the various hurricane-tornado environmental parameters presented in the tables, the mean 700-hPa wind speed, BRN shear, and helicity parameters correlate best with tornado outbreak severity, as measured by log(F sum). Because winds in landfalling hurricanes usually weaken only slowly aloft and commonly display maximum strength near 700 hPa, the postlandfall winds at that level are often roughly proportional to prelandfall hurricane intensity. Thus the sizeable correlation between 700-hPa wind speed and log(F sum) may be simply a reflection of the correlation between hurricane intensity and tornado productivity. The BRN shear and helicity parameters correlate better with log(F sum) than do simple wind differences across specific layers, probably because the latter parameters are

TABLE 12. Hurricane intensity, intensity tendency for Atlantic and Gulf landfalls.

Category	Mean intensity (m s^{-1})	Increasing	Steady	Decreasing
Gulf, tornadic	35.0	28	15	23
Gulf, nontornadic	27.9	8	7	12
Gulf, total	33.0	36	22	35
Atlantic, tornadic	36.4	7	7	10
Atlantic, nontornadic	26.2	3	9	24
Atlantic, total	30.3	10	16	34
Atlantic, total, north of SAV	30.6	7	9	25
Atlantic, total, south of SAV	29.7	3	7	9

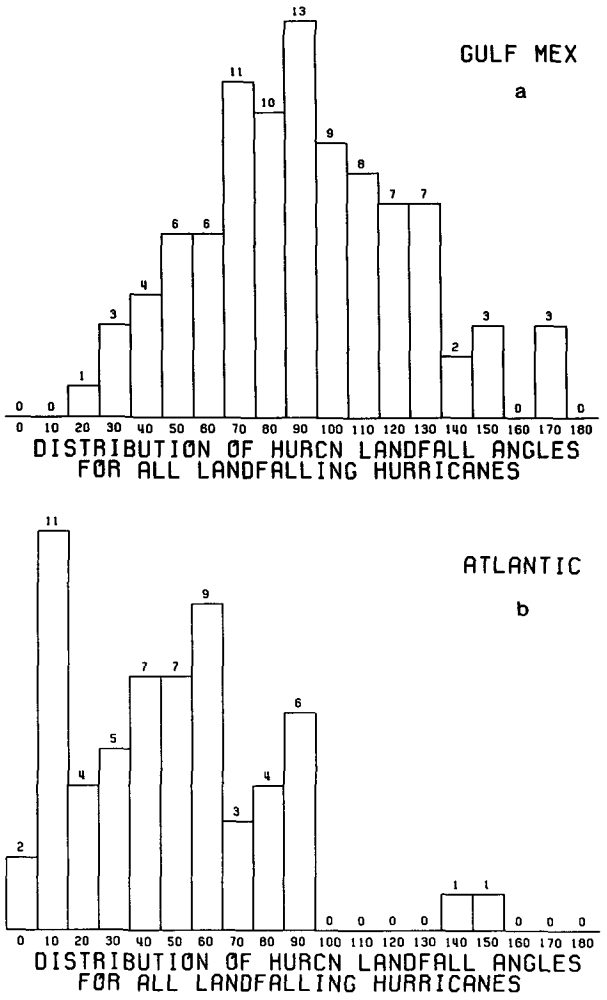

FIG. 21. Distribution of landfall incidence angles (see text for explanation) for all hurricane landfalls along (a) the Gulf of Mexico coast and (b) the Atlantic coast, during the period 1948–86. Angles were estimated to nearest 10° using smoothed coastline described in the text.

not filtered or averaged. BRN shear and helicity parameters are functions of winds at many levels in a sounding and are therefore less influenced by the effects of small-scale turbulence and measurement noise.

The BRN, often used to assess a sounding's supercell potential, appears to have some prognostic value for hurricane tornadoes. BRNs tended to be within the "possible supercell" range for many of the hurricane-tornado composites. However, considerable fluctuation was observed in this parameter for individual tornado proximity raobs, with many values smaller than 10 but others exceeding 1000 in a distribution that was skewed. In addition, it is not known what proportion of hurricane-spawned tornadoes actually come from supercell storms, which BRN was originally designed to identify. McCaul (1987) has found evidence of supercells in Hurricane Danny of 1985, where BRN values were around 20.

The fact that there is a negative correlation between CAPE and log(F sum) in the hurricane-tornado data does not prove that CAPE is unimportant or unnecessary. The negative correlation between CAPE and log(F sum) is apparently simply a reflection of the warmer anvil canopies aloft in the more intense hurricanes and does not imply lack of instability in the lower troposphere in those storms. In fact, the hurricane CAPEs are often sufficient to support updrafts of the order of 10 m s^{-1} or more, even when water loading (Seitter and Kuo 1983) is taken into account. Furthermore, the abundance of low-level moisture and absence of significant capping inversions in hurricanes makes for an environment where convective storms are readily triggered.

The fact that tornadic hurricanes tend to be embedded in sheared steering currents implies the presence of large-scale horizontal temperature gradients across the hurricanes. Mean thermal profiles in the quadrants show there is an approximate 1.0°C mean horizontal temperature difference from the left to the right sides of the hurricanes through much of the middle and upper troposphere. This horizontal temperature gradient is roughly consistent with that expected from the thermal wind relationship, given the magnitude of the shear in the steering current. The superimposed across-hurricane shears associated with the hurricane's entrainment into the weakly baroclinic westerlies appear to bear major responsibility for the enhancement of the shear and helicity (and probability of tornadic storm development) in the RF quadrant. This mechanism has not been previously identified by other hurricane tornado research efforts.

Several other raob composites also show evidence of the importance of the superimposed large-scale sheared flow on the structure of the tornadic hurricanes. The "fast" moving hurricanes tend to show stronger upper-level winds and shears than the "slow" ones. Stronger shears aloft are also found on the second day after landfall than on landfall day. These findings are consistent with the notion that as hurricanes make landfall and move farther north, they gradually become entrained into westerlies containing stronger shear, especially in the middle and upper troposphere.

In view of the fact that shear in the hurricane steering current appears to explain why the hodographs have more helicity in the RF quadrant, one might expect that as the steering current shear increases, so should the chances for tornado development. However, the dependence of tornado productivity on hurricane translational speed appears to be more complex than this. Hurricanes traveling faster than about 15 m s^{-1} exhibit reduced tornadic potential, and most of the positive correlation between hurricane forward speed and tornado output comes from hurricanes moving at speeds from 3 to 7 m s^{-1}. Thus it appears that there

is an optimum range of steering current shear. The reasons for this are unknown and are worthy of further investigation.

In general, the absorption of a hurricane into the sheared westerlies is accompanied by hurricane recurvature and northeastward acceleration. Sometimes, however, no recurvature is observed. Notable examples of tornadic hurricanes that displayed well-developed "horseshoe" hodographs but failed to recurve include Hurricanes Beulah in 1967 and Allen in 1980. In some cases this may be the result of interactions with the westerlies that are simply too transient to induce recurvature. In other cases, shear may be present in the easterlies steering the hurricane. Mechanisms that are more internal to the hurricanes themselves cannot be totally ruled out: increases in low-level inflow and mid- and upper-level outflow—from whatever cause—could also produce local enhancement of shear and helicity in the hodographs. It must be reiterated, however, that some larger scale mechanism must generally be active in order to produce the highly asymmetric mean hodograph patterns seen in Fig. 12.

Although the composites show that the mean direction of steering current shear is approximately parallel to hurricane motion, this does not prove that it always assumes that orientation in each individual case. The exact orientation of the shear likely depends on the specific synoptic scale mass and wind field configuration near each hurricane. It could differ substantially from the direction of hurricane motion in individual cases, especially when the hurricane is just beginning to encounter the westerlies.

Even though a disproportionately large number of hurricane-spawned tornadoes occurs on the day of hurricane landfall, the present data also show that some tornadoes occur well prior to landfall. In fact, some hurricanes passing close to the continent produce tornadoes without ever subsequently coming ashore. The shear enhancement caused by core cooling (Novlan and Gray 1974) is not likely to be important for tornadic storm genesis in these cases. The increase of low-level shear caused by surface drag (Gentry 1983) cannot, however, be ruled out, nor can interactions with the large-scale environmental shear.

Roughly 50% of the raobs used in this composite study came from the 18 hurricanes that spawned "major" tornado outbreaks. Development of the capability to understand and predict such major events is, of course, highly desirable. Inspection of the raob data from these major events shows nearly all conformed well to the characteristics displayed in the close-proximity composite profiles of Fig. 8. However, for weaker tornado events and for tornadoes reported in quadrants other than the RF, considerable variability of the profiles was evident. It is suspected that the variability in the reported hodographs is a reflection of the large mesoscale wind variability within and between the rainbands of hurricanes. Although the conditions favoring tornadoes are so widespread in some hurricanes that even mesoscale fluctuations cannot mask them, it appears that accurate assessment of tornado risk in marginal cases is beyond the capability of present-day standard raob practice.

Results presented here are based only on study of tornadic hurricanes. However, there are indications that some of the conclusions form a consistent picture with previously reported data on nontornadic hurricanes as well. Upper-level wind plots given by Novlan and Gray (1974) show substantially more azimuthal asymmetry in the vertical shear in tornadic hurricanes than in nontornadic ones and greater veering of winds in the tornado-prone RF quadrant. This is consistent with the present findings of significant positive correlation between the helicity parameters and tornado outbreak severity and of the systematic effect steering current shear has on hodograph shape in the various quadrants of hurricanes. Novlan and Gray (1974) also reported that tornadic hurricanes exhibited less thermodynamic instability than nontornadic hurricanes, a result that is consistent with the finding of this study that CAPE correlates negatively with tornado outbreak severity. The data given in Table 9 also suggest that hurricanes that produce only one tornado are not very different from those that produce none.

Two major hurricanes have affected the United States mainland since the final year of data used in this study. According to *Storm Data* (U.S. Dept. of Commerce 1988), Hurricane Gilbert of September 1988 produced 40 tornadoes in south and central Texas, an outbreak that qualifies as the second largest recorded to date. Preliminary inspection of the raob data most closely associated with the tornadoes shows that the hodographs are in excellent agreement with the hodograph patterns discussed in this paper. Well-developed "horseshoe" hodographs were present in the RF quadrant, especially just prior to and during Gilbert's recurvature and northeastward acceleration through central Texas. Hurricane Hugo of September 1989 produced severe damage in the Carolinas, but the number of confirmed tornadoes was apparently only two (U.S. Dept. of Commerce 1989). Although raobs indicated very strong low-level wind shears—Greensboro, North Carolina, reported 45 m s^{-1} winds at 850 hPa at 1200 UTC on 22 September—Hugo's fast translational speed during and following landfall soon placed it in the "above 15 m s^{-1}" category, which was found in subsection 3g to be unfavorable for major tornado activity. Hugo's nocturnal landfall and hasty retreat into mountainous country prior to maximum afternoon heating on 22 September may have also contributed to its low tornado productivity.

5. Summary and recommendations

The data presented here show that there are substantial differences between both the amplitudes and

vertical distributions of buoyancy and shear in hurricane and Great Plains tornado environments. The hodographs of tornadic hurricanes show significant differences from quadrant to quadrant, relative to hurricane motion. Shear and helicity are most favorable for tornadoes in the RF quadrant and least favorable in the LR quadrant, a fact that is well-correlated with observed tornado frequency. This variation in hodograph shape appears to be the result mainly of a superimposed across-hurricane shear in the steering current.

Although it is clear that hurricane intensity is an important factor in tornado productivity, raob data are lacking in the core regions of hurricanes, where intensity differences are most clearly manifest. Such data are needed to help explain why there are two apparently distinct modes of tornadoes—core and outer rainband—in hurricanes. Hurricane size is also important, but reliable ROCI data are not reported in the archived Atlantic hurricane track dataset. More detailed study of the relationship between tornado productivity and hurricane intensity and size would almost certainly be useful to hurricane-tornado forecasters.

Because of the small size of hurricane cores relative to the spacing of the synoptic raob network and the difficulty of launching rawinsondes under hurricane conditions, it is unlikely that an adequate sample of core raobs in landfalling hurricanes will become available anytime soon. A proper investigation of the environmental conditions accompanying core tornadoes must therefore await the installation of remote sensing equipment such as Doppler radars. Acquisition of in situ rawinsonde data by mobile launch crews (Bluestein et al. 1988; 1989; Rust et al. 1990) may provide additional insights about the conditions near tornadoes occurring in the less rigorous environment of the outer rainbands.

Doppler velocity data acquired opportunistically during the nearby passage of tornadic hurricanes will undoubtedly shed light on the structure of the tornadic storms. However, if the storms are regularly as small and shallow as those that occurred in Hurricane Danny (McCaul 1987), then the mesocyclone signatures may not be detectable unless the tornadic storms are quite close to the radar. In this case, diagnosis of probable tornadic activity might have to be made by relying on the more gross characteristics of individual echoes or echo bands and clusters. For this reason, additional case studies of the reflectivity patterns that have characterized past major hurricane-tornado outbreaks are still desirable.

The data presented here are limited only to tornado-proximal raobs observed in hurricane environments. Although it is suspected that some of the present findings, such as the strongly asymmetric distribution of helicity and hodograph curvature around the hurricanes, hold true to some extent even for nontornadic hurricanes, it would be desirable to extend this study to cover all landfalling hurricanes. In addition, the present work could be extended to include a study of all available prelandfall sounding profiles from tornado-producing hurricanes in order to see if there exist any precursor signals that might be helpful in predicting the tornado activity.

This study has shown that there are statistically significant correlations between hurricane-tornado outbreak intensity and meteorological parameters such as vertical shear and layer averages of helicity and streamwise vorticity. Unfortunately, the correlations, though statistically significant, are too small to qualify individually as definitive prediction aids in forecasts of the intensity of hurricane-tornado activity. Consideration of the totality of factors examined in this study—hurricane size, intensity and forward speed, hodograph helicity and shear, presence of at least some buoyancy, location and timing of landfall—may yield improved forecasts. Some additional improvement may be seen once a large enough database is obtained so that thorough and detailed stratifications of the data against the above factors can be performed. Ultimately, however, adequate account must be taken not only of point values of parameters furnished by individual soundings, but also of the gradients and temporal changes of those parameters. A substantial amount of additional observational and numerical simulation work will be needed in order to expand and refine our understanding of the important details of the mesoscale organization within landfalling hurricanes and of the ways hurricanes interact with the flow in a sheared environment.

Acknowledgments. Part of this work was done in conjunction with the author's dissertation research at the University of Oklahoma, under the auspices of NSF Grant ATM-850130. Considerable elaboration and refinement of the results were accomplished during the author's tenure as an Advanced Study Program postdoctoral fellow at NCAR's Mesoscale and Microscale Meteorology Division. The author wishes to thank Doug Lilly, Howie Bluestein, Bob Davies-Jones, Rich Rotunno, Gary Barnes, Morris Weisman, Ed Zipser, Kerry Emanuel, Joe Klemp, Don Burgess, Bill Gray, and anonymous reviewers for many helpful discussions and suggestions made during the course of this work. Other useful discussions were had with Claude Duchon and John Flueck. The hurricane data tape was obtained from the National Climatic Data Center, Asheville, North Carolina. The National Severe Storms Forecast Center, Kansas City, Missouri, furnished a copy of its tornado data tape. Will Spangler provided the software needed to extract the raob data from the NCAR time series raob data tapes. The hurricane and tornado tapes and raob data were analyzed on the University of Oklahoma IBM 3081K mainframe and Geosciences Computing Network VAX 11/785. Additional analyses were accomplished at NCAR, using both the Cray X/MP-48 and the MMM VAX 8550. Ken Hansen,

Pat Waukau, Bill Boyd, and other NCAR consultants helped in the transfer and adaptation of data and software. Some final calculations were performed on the Space Science Laboratory VAX 11/785 at Marshall Space Flight Center, Huntsville, Alabama, under NASA Grant NASA8-37135.

REFERENCES

Barnes, G. M., E. J. Zipser, D. Jorgensen and F. Marks, Jr., 1983: Mesoscale and convective structure of a hurricane rainband. *J. Atmos. Sci.*, **40,** 2125–2137.

——, and G. J. Stossmeister, 1986: The structure and decay of a rainband in Hurricane Irene (1981). *Mon. Wea. Rev.*, **114,** 2590–2601.

Bluestein, H. B., and M. H. Jain, 1985: Formation of mesoscale lines of precipitation: Severe squall lines in Oklahoma during the spring. *J. Atmos. Sci.*, **42,** 1711–1732.

——, E. W. McCaul, Jr., G. P. Byrd and G. R. Woodall, 1988: Mobile sounding observations of a tornadic thunderstorm near the dryline: The Canadian, Texas, storm of 7 May 1986. *Mon. Wea. Rev.*, **116,** 1790–1804.

——, ——, ——, ——, G. Martin, S. Keighton and L. C. Showell, 1989: Mobile sounding observations of a thunderstorm near the dryline: The Gruver, Texas, storm complex of 25 May 1987. *Mon. Wea. Rev.*, **117,** 244–250.

Darkow, G. L., and D. W. McCann, 1979: Relative environmental winds for 121 tornado bearing storms. Preprints, *11th Conf. Severe Local Storms,* Kansas City, Amer. Meteor. Soc., 413–417.

Davies-Jones, R., 1984: Streamwise vorticity: The origin of updraft rotation in supercell storms. *J. Atmos. Sci.*, **41,** 2991–3006.

Davies-Jones, R., D. Burgess and M. Foster, 1990: Test of helicity as a tornado forecast parameter. Preprints, *16th Conf. Severe Local Storms,* Kananaskis, Alberta, Amer. Meteor. Soc., 588–592.

Dixon, W. J., and F. J. Massey, Jr., 1969: *Introduction to Statistical Analysis.* McGraw-Hill, 638 pp.

Doswell, C. A., and D. W. Burgess, 1988: On some issues of United States tornado climatology. *Mon. Wea. Rev.*, **116,** 495–501.

Frank, W. M., 1977: The structure and energetics of the tropical cyclone. I: Storm structure. *Mon. Wea. Rev.*, **105,** 1119–1135.

Fujita, T. T., 1973: Tornadoes around the world. *Weatherwise,* **26,** 56–83.

——, K. Watanabe, K. Tsuchiya and M. Shimada, 1972: Typhoon-associated tornadoes in Japan and new evidence of suction vortices in a tornado near Tokyo. *J. Meteorol. Soc. Jpn.*, **50,** 431–453.

Gentry, R. C., 1983: Genesis of tornadoes associated with hurricanes. *Mon. Wea. Rev.*, **111,** 1793–1805.

Hawkins, H. F., and S. M. Imbembo, 1976: The structure of a small, intense hurricane—Inez 1966. *Mon. Wea. Rev.* **104,** 418–442.

Hill, E. L., W. Malkin and W. A. Schulz, Jr., 1966: Tornadoes associated with cyclones of tropical origin—practical features. *J. Appl. Meteor.*, **5,** 745–763.

Jordan, C. L., 1958: Mean soundings for the West Indies area. *J. Meteor.*, **15,** 91–97.

Kelly, D. L., J. T., Schaefer, R. P., McNulty, C. A. Doswell III and R. F. Abbey, 1978: An augmented tornado climatology. *Mon. Wea. Rev.* **106,** 1172–1183.

Lilly, D. K., 1986: The structure, energetics, and propagation of rotating convective storms. Part II: Helicity and storm stabilization. *J. Atmos. Sci.*, **43,** 126–140.

Maddox, R. A., 1976: An evaluation of tornado proximity wind and stability data. *Mon. Wea. Rev.* **104,** 133–142.

McCaul, E. W., Jr., 1987: Observations of the Hurricane "Danny" tornado outbreak of 16 August 1985. *Mon. Wea. Rev.*, **115,**1206–1223.

Merrill, R. T., 1983: A comparison of large and small tropical cyclones. *Mon. Wea. Rev.*, **112,** 1408–1418.

Novlan, D. J., and W. M. Gray, 1974: Hurricane-spawned tornadoes. *Mon. Wea. Rev.* **102,** 476–488.

Powell, Mark D., 1990: Boundary layer structure and dynamics in outer hurricane rainbands. Part I: Mesoscale rainfall and kinematic structure. *Mon. Wea. Rev.*, **118,** 891–917.

Rust, W. D., D. W. Burgess, R. A. Maddox, L. Showell, T. C. Marshall and D. K. Lauritsen, 1990: Testing a mobile version of a Cross-Chain Loran Atmospheric (M-CLASS) Sounding System. *Bull. Amer. Meteor. Soc.*, **71,** 173–180.

Schaefer, J. T., and R. L. Livingston, 1988: The typical structure of tornado proximity soundings. *J. Geophys. Res.*, **93,** 5351–5364.

Seitter, K. L., and H.-L. Kuo, 1983: The dynamical structure of squall-line type thunderstorms. *J. Atmos. Sci.*, **40,** 2831–2854.

Sheets, R. C., 1969: Some mean hurricane soundings. *J. Appl. Meteor.*, **8,** 134–146.

U.S. Dept. of Commerce, 1987: Tropical Cyclones of the North Atlantic Ocean, 1871–1986, C. J. Neumann, Ed., 186 pp. [Available from National Climatic Data Center, Asheville, NC.]

U.S. Dept. of Commerce, 1988: *Storm Data,* **30**(9), 56 pp.

U.S. Dept. of Commerce, 1989: *Storm Data,* **31**(9), 64 pp.

Weisman, M. L., and J. B. Klemp, 1982: The dependence of numerically simulated convective storms on vertical wind shear and buoyancy. *Mon. Wea. Rev.*, **110,** 504–520.

——, and ——, 1984: The structure and classification of numerically simulated convective storms in directionally varying shears. *Mon. Wea. Rev.*, **112,** 2479–2498.

Weiss, S. J., 1985: On the operational forecasting of tornadoes associated with tropical cyclones. Preprints, *14th Conf. Severe Local Storms,* Indianapolis, Amer. Meteor. Soc., 293–296.

——, 1987: Some climatological aspects of forecasting tornadoes associated with tropical cyclones. Preprints, *17th Conf. Hurr. and Trop. Meteor.*, Miami, Amer. Meteor. Soc., 160–163.

Willoughby, H. E., F. D. Marks, Jr. and R. J. Feinberg, 1984: Stationary and moving convective bands in hurricanes. *J. Atmos. Sci.*, **41,** 3189–3211.